CEBAF Program Advisory Committee Six (PAC6) Proposal Cover Sheet

This proposal must be received by close of business on April 5, 1993 at:

CEBAF
User Liaison Office
12000 Jefferson Avenue
Newport News, VA 23606

Proposal Title

Electroproduction of Light Quark Mesons

Contact Person

Name: Mikhail V.Kossov
Institution: CEBAF
Address: 12000 Jefferson Avenue
Address: Physics Department MS 12H
City, State ZIP/Country: Newport News, VA 23606
Phone: (804) 249-7175 **FAX:** (804) 249-5800
E-Mail → BITnet: CEBAF::KOSSOV **Internet:**KOSSOV@CEBAF.gov

If this proposal is based on a previously submitted proposal or letter-of-intent, give the number, title and date:

CEBAF Use Only

Receipt Date: 4/5/93 Log Number Assigned: PR 93-012

By: gp

Electroproduction of Light Quark Mesons

Spokesperson: M.Kossov

The M* Group in the CLAS Collaboration:

V.Burkert, D.Joyce, B.Mecking, M.Mestayer, B.Niczyporuk, E.S.Smith
CEBAF, Newport News, Virginia

M.Kossov
Institute of Theoretical and Experimental Physics, Moscow, Russia
and
Christopher Newport University, Newport News, Virginia

P.Degtyarenko
Institute of Theoretical and Experimental Physics, Moscow, Russia
and
University of Massachusetts, Amherst, Massachusetts

N.Pivnyuk
Institute of Theoretical and Experimental Physics, Moscow, Russia

A.Klein, S.Kuhn, L.Weinstein
Old Dominion University, Norfolk, Virginia

L.Elouadrhiri, R.S.Hicks, R.Miskimen, G.A.Peterson, K.Wang
University of Massachusetts, Amherst, Massachusetts

D.Doughty, D.Heddle, Z.Li
Christopher Newport University, Newport News, Virginia

H.Funsten
College of William and Mary, Williamsburg, Virginia

(Proposal is open for collaboration)

ABSTRACT

We propose to measure the Q^2-dependence of the electroproduction of mesons in the reaction $ep \rightarrow e'pM^*$. This measurement permits a determination of the Q^2-dependence of the transition form-factors for mesons ($\gamma\pi M^*$ vertex). Two-quark systems are easier to calculate than three-quark system and therefore the meson transition form-factors, which are very sensitive to the meson structure, allow to test various quark models. For example, in the framework of non-relativistic model, the form-factors provide constraints for the $q\bar{q}$ wave functions. To separate the contribution of the One Pion Exchange mechanism, a comparative analysis of the production of the resonances with I=0 and with I=1 is proposed. At electron energies up to 3 GeV, one can investigate the $^3S_1$ states of the $q\bar{q}$ system (ρ and ω mesons). The measurement of the $\rho\omega$ mixing in the $\pi^+\pi^-$ decay channel permits a determination of the fundamental value of the mass difference of light quarks. Due to its high statistical accuracy, the $ep \rightarrow e'p\pi^+\pi^-$ reaction can be used to analyze the angular correlations in the $\pi^+\pi^-$ decay of ρ meson. This measurement of the ρ polarization permits a determination of the spin-flip amplitude in the diffractive vector meson electroproduction. At energies up to 4 GeV it is possible to investigate the transition form-factors for $^1P_1$, $^3P_0$, $^3P_1$, $^3P_2$, and 2^3S_1 states of the $q\bar{q}$ system which are all known to exist. Future upgrades of the CEBAF accelerator (energy up to 6 GeV) will allow to study $^3D_1$,$^3D_2$, $^3D_3$, and $^1D_2$ states of the $q\bar{q}$ system, half of which have not yet been discovered. The combination of the high quality CEBAF beam and the large acceptance of the CLAS detector makes it possible to measure the Q^2-dependence of the transition form-factors up to 2 GeV^2 at 4 GeV and up to 4 GeV^2 at 6 GeV.

1. Introduction

The non-relativistic quark model with QCD-inspired improvements successfully describes the properties of the known mesons [1]. For the description of the meson mass spectrum the One Gluon Exchange Potential is used. The potential is shown in Fig.1. At short distances it is similar to the Coulomb potential, and at long distances the potential is defined by the color string energy. The masses of heavy quark mesons are only sensitive to the "Coulomb like" part of the potential while the masses of light quark mesons are sensitive to the "confinement" part of the potential. The higher the radial excitation of the meson, the larger the radius of quark-quark interaction. In the framework of this potential model, predictions can be made for the Q^2-dependence of $F_{\pi\to M^*}$ transition form-factors for different radial excitations of mesons. According to the Cabibbo-Radicati sum rule for mesons [2], the form-factors for ρ, ω, and ϕ mesons decrease with Q^2, and the form-factors of P-, 2S-, and D-wave mesons increase in such a way that the sum of the form-factors is independent of Q^2. As a result of this behavior heavy resonance production dominates at large Q^2.

Table 1. Light Quark Mesons

Meson	J^{PC}	I=0	m,MeV	Γ,MeV	I=1	m,MeV	Γ,MeV	$s\bar{s}$	m,MeV	Γ,MeV
1^1S_0	0^{-+}	η	547.5	1.2	π	137.		η'	975.3	0.2
1^3S_1	1^{--}	ω	782.	8.4	ρ	768.1	151.5	ϕ	1019.	4.4
1^1P_1	1^{+-}	h_1	1170.	360.	b_1	1232.	155.	h_1'	1380.	80.
1^3P_0	0^{++}	f_0	974.1	47.	a_0	982.7	57.	f_0'	1400.	270.
1^3P_1	1^{++}	f_1	1282.	24.	a_1	1260.	400.	f_1'	1426.	56.
1^3P_2	2^{++}	f_2	1275.	185.	a_2	1318.	110.	f_2'	1525.	76.
2^3S_1	1^{--}	ω'	1394.	229.	ρ'	1465.	310.	ϕ'	1680.	150.
1^1D_2	2^{-+}				π_2	1670.	250.			
1^3D_1	1^{--}	ω_1	1594.	100.	ρ_1	1700.	235.			
1^3D_2	2^{--}									
1^3D_3	3^{--}	ω_3	1668.	166.	ρ_3	1691.	215.	ϕ_3	1854.	87.

The diagrams relevant for the production of light quark mesons are shown in Fig.2. The experiment is aimed at the investigation of the $\gamma\pi M^*$ vertex (Fig.2a). The first cut for the isolation of this process is $-t < M^2$ (M is the mass of the produced meson). At large $-t$, heavy meson exchange and N^* formation in the s-channel diagrams (Fig.2c,d) dominate. The contribution of these diagrams, which are difficult to separate, to the reaction amplitude can be expressed by a dual diagram Fig.2e. Note that there exists an already approved CLAS proposal 91-024 aimed at the search for "Missing" Resonances in the Electroproduction of Omega

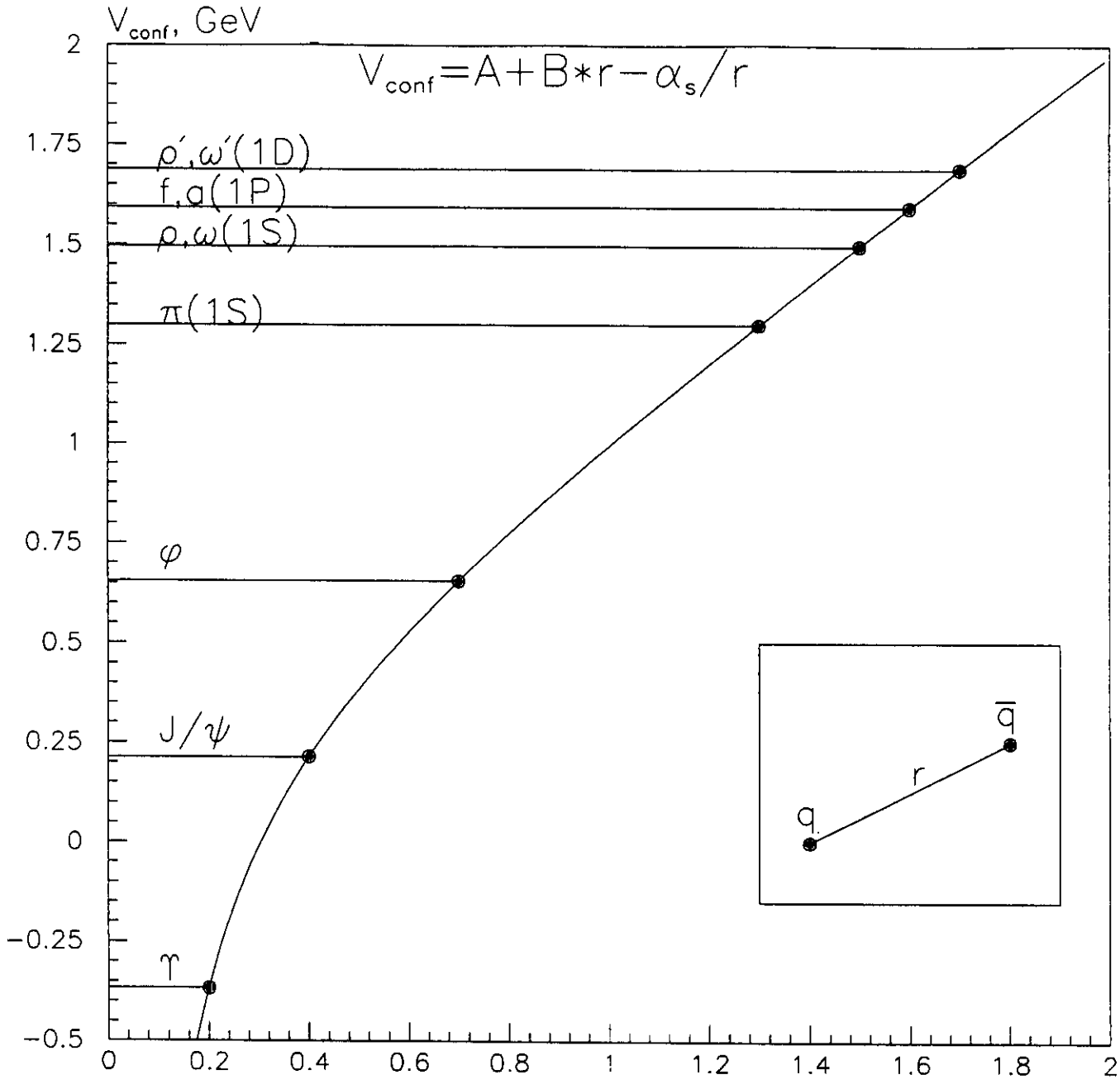

Fig.1. One Gluon Exchange Potential.

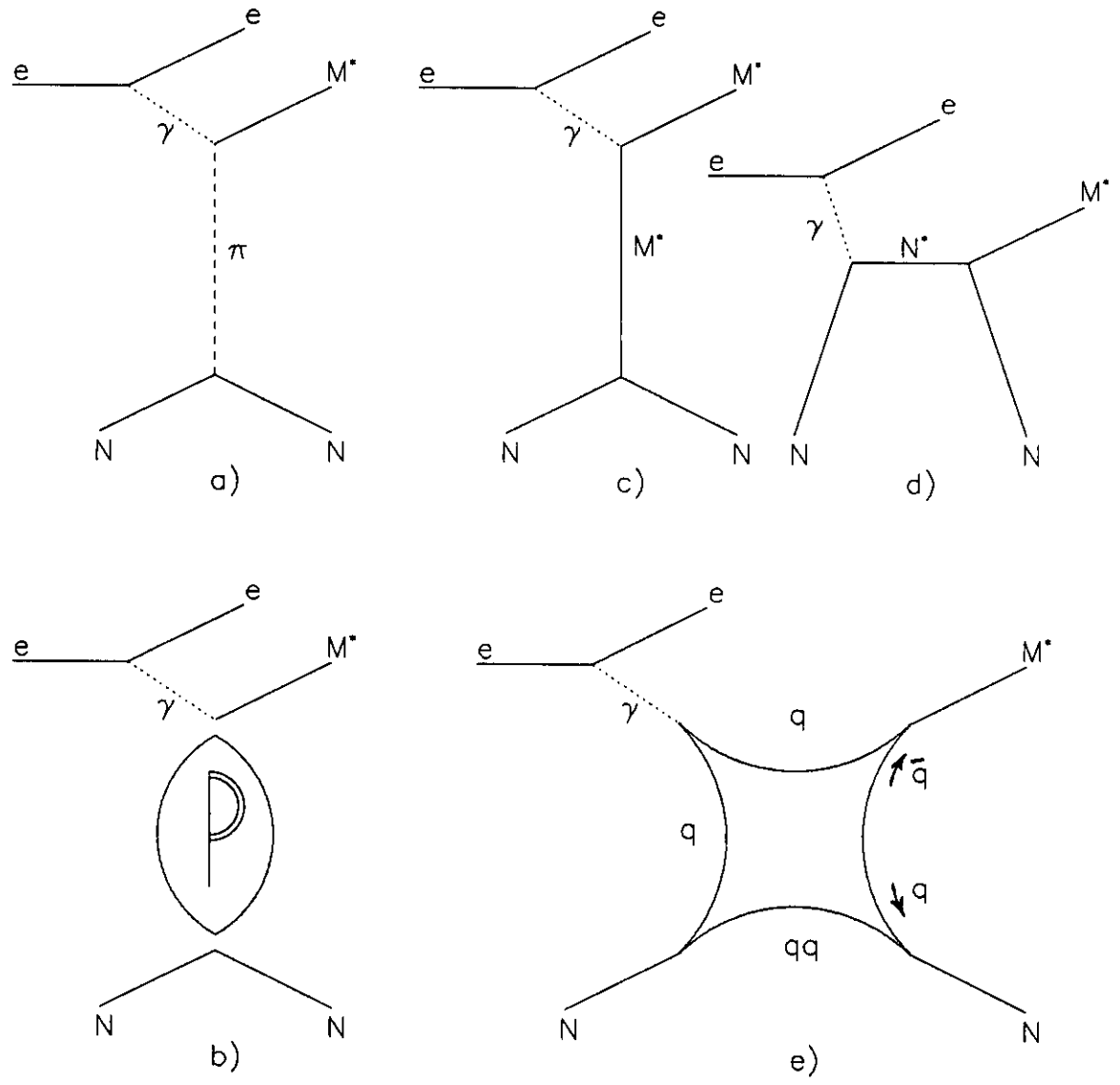

Fig.2. Feinman Diagrams for Meson Electroproduction

Mesons. This experiment will analyze events in the kinematical region where these dual diagrams dominate.

To study the transition form-factors $F_{\pi \to M^*}$ as a function of Q^2, it is necessary to separate the diffractive from the One Pion Exchange (OPE) contributions. It is necessary only for $^1S_1(1^{--})$ and $^3D_1(1^{--})$ states for which a diffractive contribution is possible. In the first case, the $\rho(768)(I=1)$ and $\omega(782)(I=0)$ mesons and in the second case the $\rho(1700)(I=1)$ and $\omega(1594)(I=0)$ mesons should be analyzed. The dominant decay modes for these mesons are $n\pi$ modes: $\pi^+\pi^-$ for the ρ-meson, $\pi^+\pi^-\pi^o$ for the ω-meson, 4π for the $\rho(1700)$-meson and $\pi^+\pi^-\pi^o$ and $2\pi^+2\pi^-\pi^o$ modes for the $\omega(1594)$-meson. It should be noted that it is not necessary to detect four mesons in case of the 5-pion decay of $\omega(1594)$-meson because $\pi^+\pi^-\pi^o$ mesons are a product of the ω-meson decay, and the ω-meson can be detected by determining the missing mass in the $ep \to e'p\pi^+\pi^-(\omega)$ reaction.

In Appendix A it is shown that the diffractive contribution to the production of isovector mesons is nine times larger than the diffractive contribution to the production of isoscalar mesons. In contrast, the OPE contribution to the production of isovector mesons is nine times less than the OPE contribution to the production of isoscalar mesons. It is known experimentally that the contributions of the diffraction and the OPE mechanism are comparable for isoscalar mesons and hence one can neglect the OPE contribution for isovector meson production. As a result the OPE contribution in the kinematical region, where OPE and diffraction dominate, may be estimated as $\sigma^{OPE} = \sigma^{I=0} - \frac{1}{9}\sigma^{I=1}$. This method can be used to subtract the diffractive contribution for isoscalar/isovector meson production.

The Q^2 range, which is interesting for the transition form factors, can be estimated in the framework of the naive quark model. If the initial $q\bar{q}$ state is considered to be two quark state with the quark masses $\mu_q = .33GeV/c^2$, and in the final state one quark acquires an energy E_q (Fig.3a) then the squared mass of the final state meson can be calculated as $M^2 = (p_{1in} + p_{2fin})^2 = 2\mu_q^2 + 2\mu_q E_q$ and the transferred momentum as $-Q^2 = (p_{2fin} - p_{2in})^2 = 2\mu_q^2 - 2\mu_q E_q$. Then one can find that $Q^2 = M^2 - 0.4$ and, in accordance with this estimate, the P-wave mesons $(M = 1.27GeV/c^2)$ should dominate at $Q^2 = 1.2GeV^2$, and the D-wave mesons $(M = 1.68GeV/c^2)$ should dominate at $Q^2 = 2.4GeV^2$.

The Q^2 dependence can be estimated more precisely using the oscillator potential model for mesons. In this case the dual sum of the cross sections of the electroproduction of different mesons can be considered as an interaction with only one quark of $q\bar{q}$ pair (Fig.3a). According to the Cabibbo-Redicati sum rule for mesons the sum of meson production cross sections $\Sigma d\sigma_i^M/dQ^2$ equals the sum over the quarks in the meson $\Sigma e_j^2 d\sigma_j^q/dQ^2$. If one normalizes the meson production cross section to the sum of quark cross sections then the Q^2-dependence for S-wave mesons is expected to decrease exponentially with Q^2: $(d\sigma^S/dQ^2/\Sigma e_j^2 d\sigma_j^q/dQ^2) = exp(-\frac{Q^2}{8\beta^2})$, where β=0.3 GeV is the parameter of the oscillator potential. For P-wave mesons

Fig.3. Transition form-factors of radially excited mesons

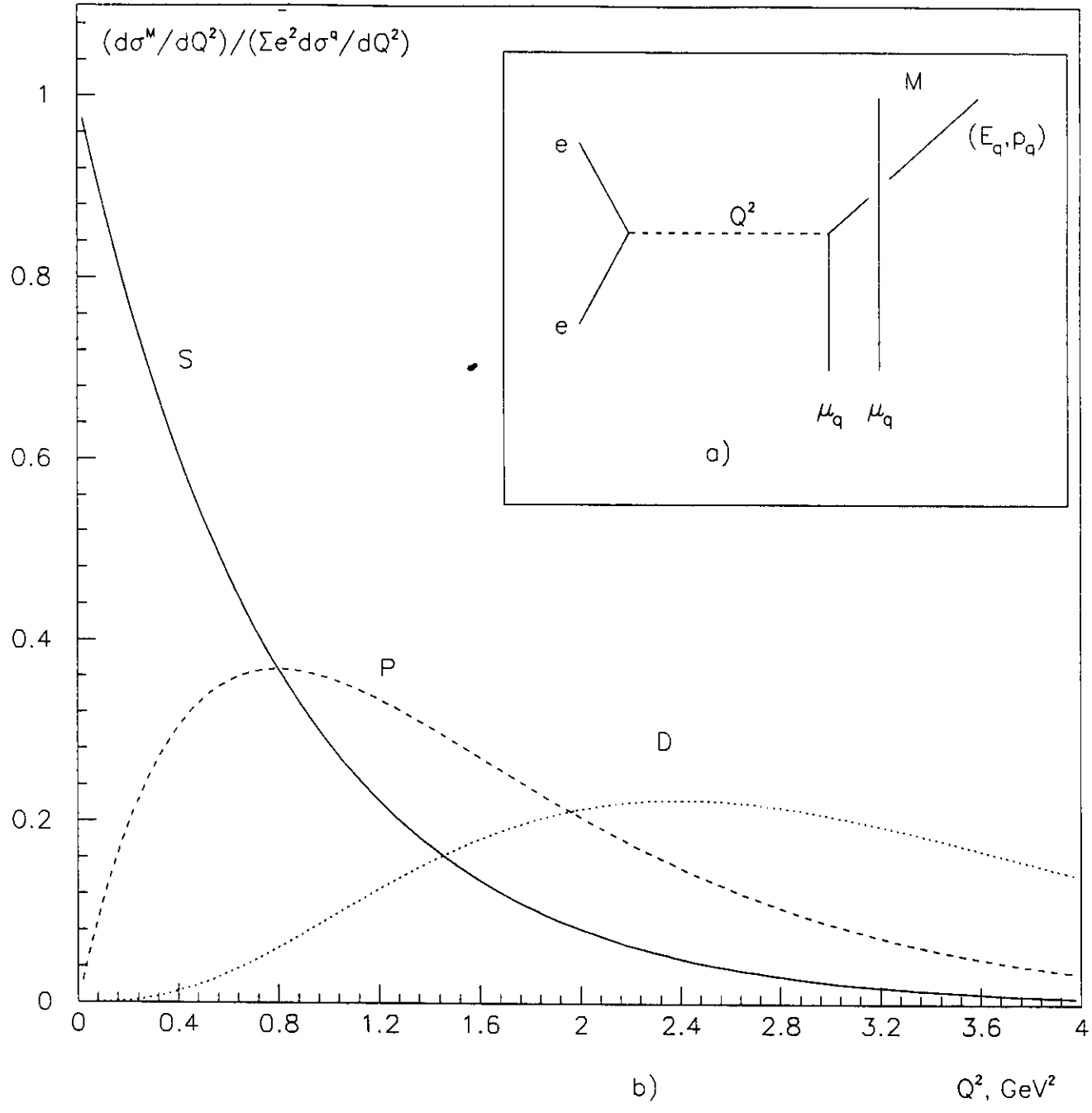

the transition form-factor is proportional to $\frac{Q^2}{8\beta^2}exp(-\frac{Q^2}{8\beta^2})$, and for D-wave mesons it is proportional to $(\frac{Q^2}{8\beta^2})^2exp(-\frac{Q^2}{8\beta^2})$. Since the sum of all these terms should be equal to unit, the coefficients of the proportionality can be easily found as an expansion of the exponent. The resulting Q^2dependence of the transition form-factors is illustrated in Fig.3b. The estimated Q^2 regions where different radial excitations of meson dominate agree with the estimates of the naive quark model.

The kinematics of meson production is considered in Appendix B. The electron acceptance of the CLAS detector for the beam energies 2, 3, 4, and 6 GeV is shown in Fig.4 for the full field of the toroidal magnet (dashed lines). With the magnetic field reduced by a factor two the Q^2 threshold is reduced by the same factor. In the same figure one can see the thresholds for the production of S-, P-, and D-wave mesons (solid lines, the kinematical regions of the reaction are to the right of these lines). One can see that the CLAS acceptance covers the kinematical region where P- and D-resonances are expected to be dominant. The diagrams of the intermediate N^* production mechanism and heavy meson exchange (Fig.2c,d) dominate at large $-t$. The $-t = M^2$ kinematical boundary (dotted line in Fig.4) can be considered as an additional constraint for the kinematical region of the reaction.

The comparison of the kinematical restrictions and the detector acceptance shows that, at electron energies less then 3 GeV, it is possible to investigate $^3S_1$ states of $q\bar{q}$ system (ρ, ω - see Tab.1) only, at energies up to 4 GeV it becomes possible to investigate $^1P_1$, $^3P_0$, $^3P_1$, $^3P_2$, and 2^3S_1 states all of which are presently known. A future upgrade of the CEBAF accelerator (up to the energy 6 GeV) will allow to study $^3D_1$, $^3D_2$, $^3D_3$, and $^1D_2$ states half of which have not yet been discovered (Tab.1).

2. Existing Data

There are a number of papers describing the investigation of photo- and electroproduction of mesons: (S-states) ρ and ω mesons production [3-17], (P-states) a, b and h mesons production [18-19], and (D-states) ρ' and ω' mesons production in [20-28]. In the recent work of Condo et al. (channels $\gamma p \to n\pi^+\pi^+\pi^-$ and $\gamma p \to p\pi^+\pi^+\pi^-\pi-$) an interesting $q\bar{q}$ state $\pi(1775)1^-(?^{-+})$ has been found. This finding requires confirmation.

For the photo- and electroproduction of ρ and ω mesons, the only existing model was developed by H.Fraas [31]. The diffractive production was parametrized in [30]; later, an accurate consideration of the phase shift analysis was done in [32]. This model was used for data analysis in most experiments that measured the cross sections of photo- or electroproduction of mesons. Later, the form-factors F_N and F_ω for $N\pi N$ an $\gamma\pi\omega$ vertices respectively were introduced [7]. Details of the model are described in Appendix C.

Fig.4. Kinematical regions for meson production in CLAS

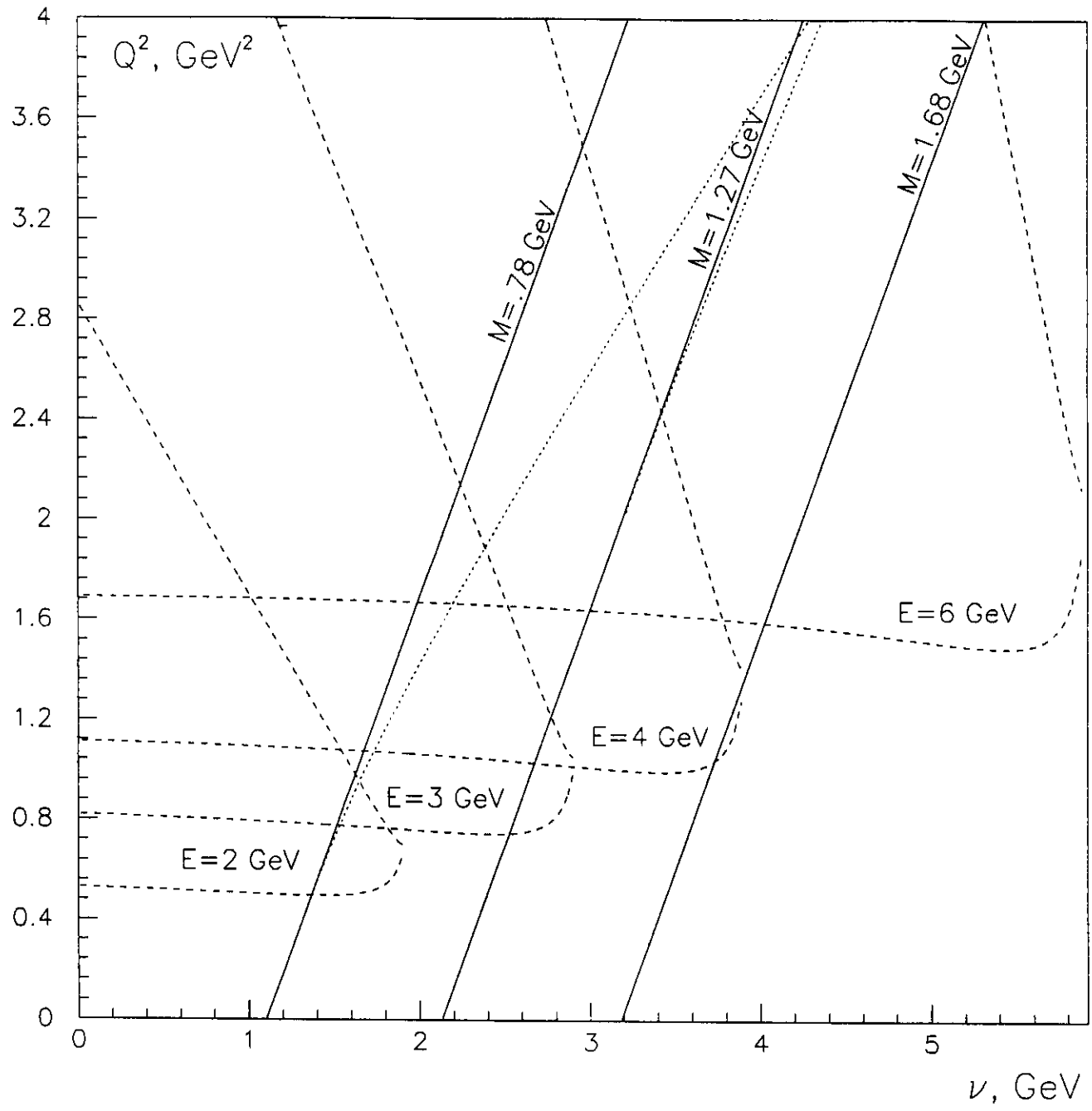

The diffractive part of the model has been tested in [16] where exclusive ρ^0 production has been investigated in deep inelastic muon-proton scattering. The Q^2-dependence of the reaction is shown in Fig.5. In [16] the old version of the model [30] was used for the analysis. The solid line in the figure corresponds to the prediction of the model. The dashed line corresponds to the transverse part of the cross section only. The comparison of the experimental data with the model calculations shows that the longitudinal part of the cross section is less than predicted by the model. The description of the same data with the new version of the model [31,7] is shown in the same figure. The calculated curve (dotted line in Fig.5) comes close to the experimental data, but the cross section without longitudinal contribution (dash-dotted line in Fig.5) still describes the data much better, especially for large Q^2.

The analysis of the ρ meson polarization shows that, at large Q^2, the ρ meson becomes longitudinal ($cos^2(\theta)$-like angular distribution of the secondary pions - Fig.6a). In Fig.6b, the Q^2 dependence of the ρ polarization is shown. At present this anomalous effect (high spin-flip amplitude in ρ-meson electroproduction at large Q^2) is not explained.

In the decay channel $M^* \rightarrow \pi^+\pi^-$, the $\rho\omega$ mixing can be studied. In Fig.7 the effect of $\rho\omega$ mixing is demonstrated [33]. Experiments on the $\rho\omega$ mixing demand high statistics, therefore most experiments have been carried out in inclusive M^* production on nuclei [33,34].For the analysis of the $\rho\omega$ mixing the ρ meson propagator $\frac{1}{M^2-m_\rho^2+i\Gamma m_\rho}$ has to be replaced by the mixing propagator

$$\frac{1}{M^2-m_\rho^2+i\Gamma m_\rho}+\frac{\zeta e^{i\chi}}{M^2-m_\omega^2+i\Gamma m_\omega}.$$

The result of the description by the mixing propagator is shown in Fig.7. The fit to the data corresponds to the parameters $\zeta = 0.01$ and $\chi = 100^o$. These parameters are significant for determining the mass difference of light quarks [35]. Only a small part of the $\rho\omega$ mixing is due to the $\omega - \gamma - \rho$ transition while the bulk of the effect is caused by the mass difference between u and d quarks. As was shown in [35], the $\rho\omega$ mixing in photoproduction is one of the clearest ways to determine the quark mass difference.

3. Proposed Experiment

3.1 Isolation of Meson Resonances

We propose to detect all charged final state particles in meson production reaction (Tab.2). One residual neutral hadron can be reconstructed using a missing mass distribution. When a final state baryon is reconstructed as a missing mass

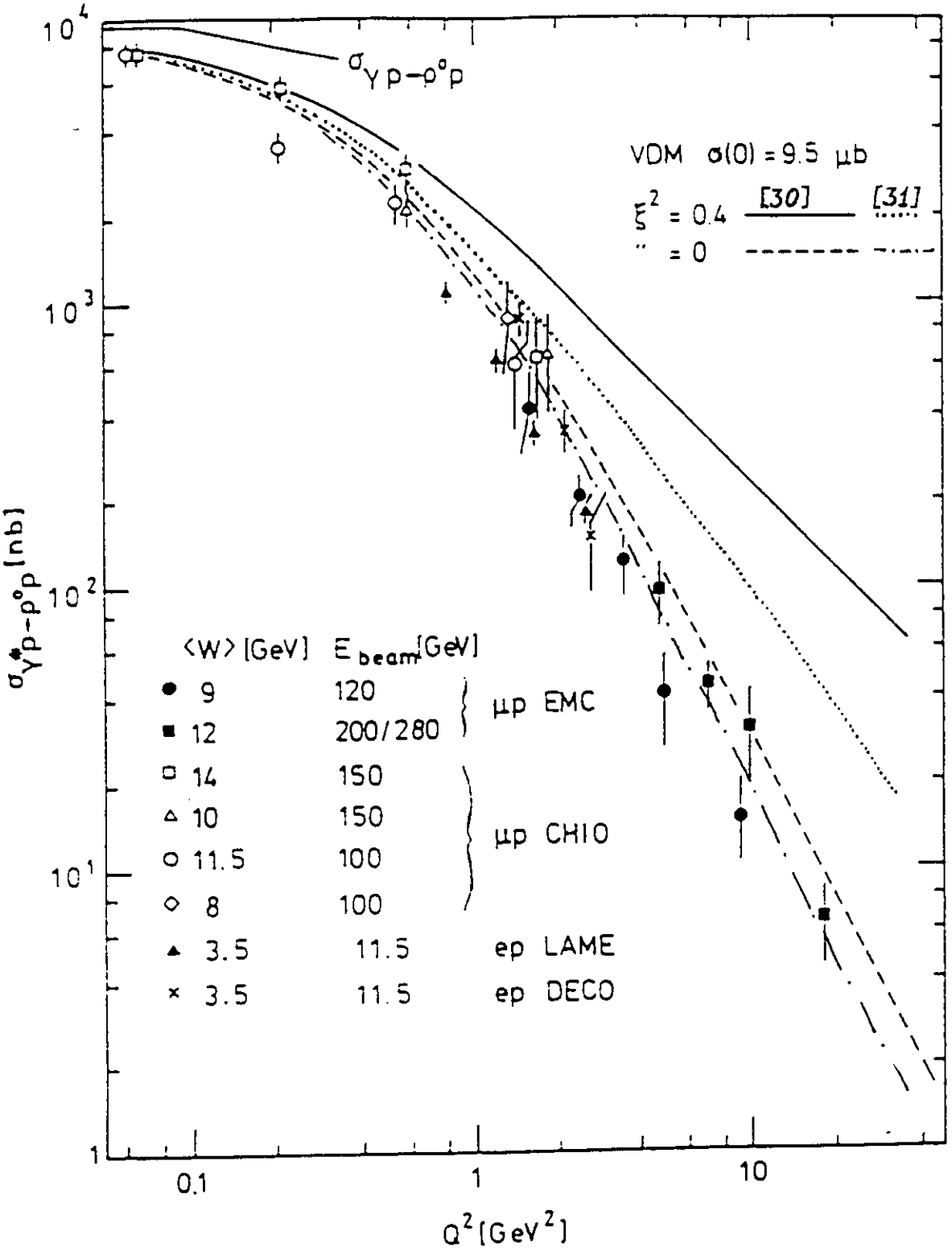

Fig.5. Q^2 dependence of ρ meson electroproduction

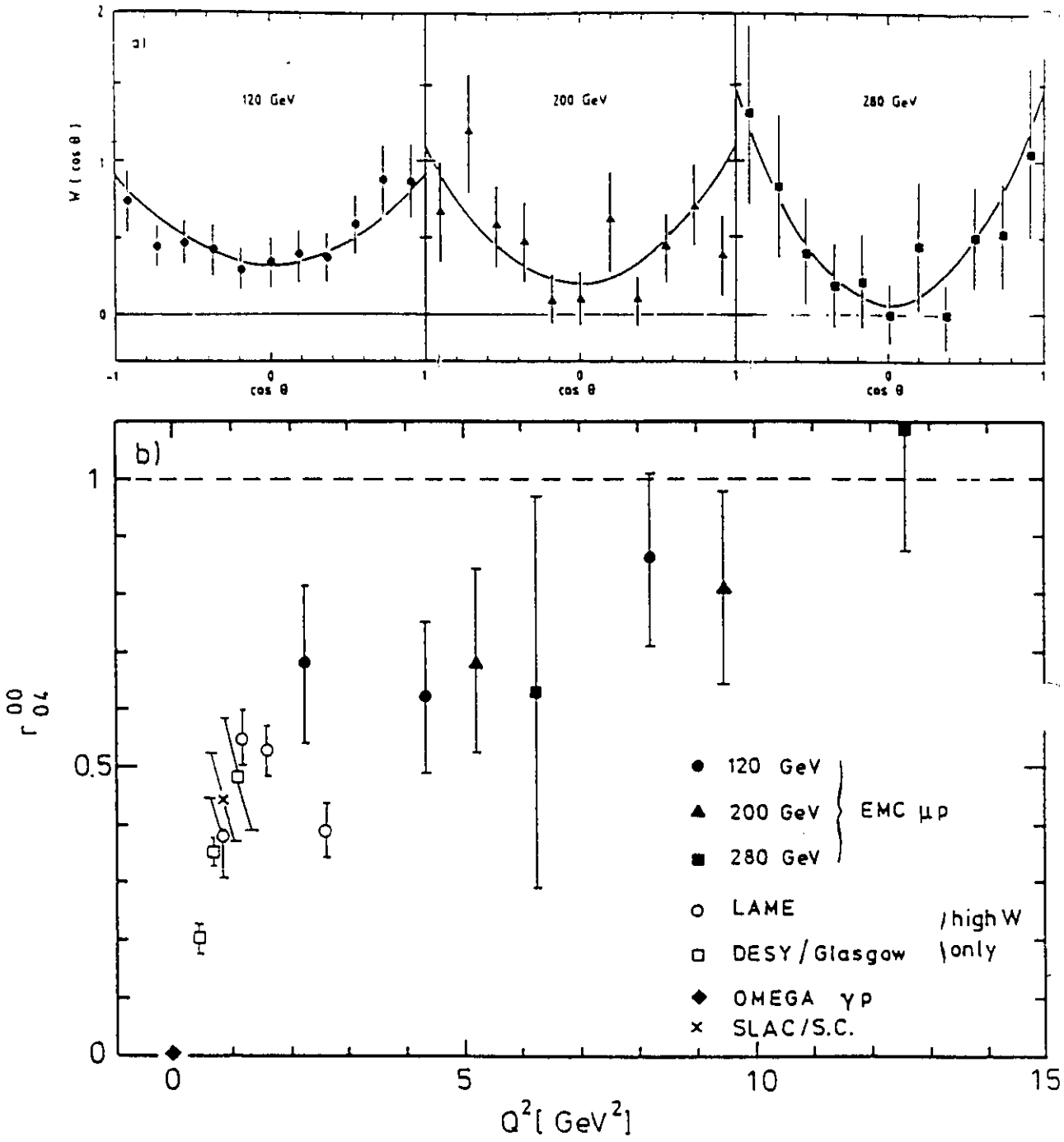

Fig.6. Polarization of electroproducted ρ–mesons

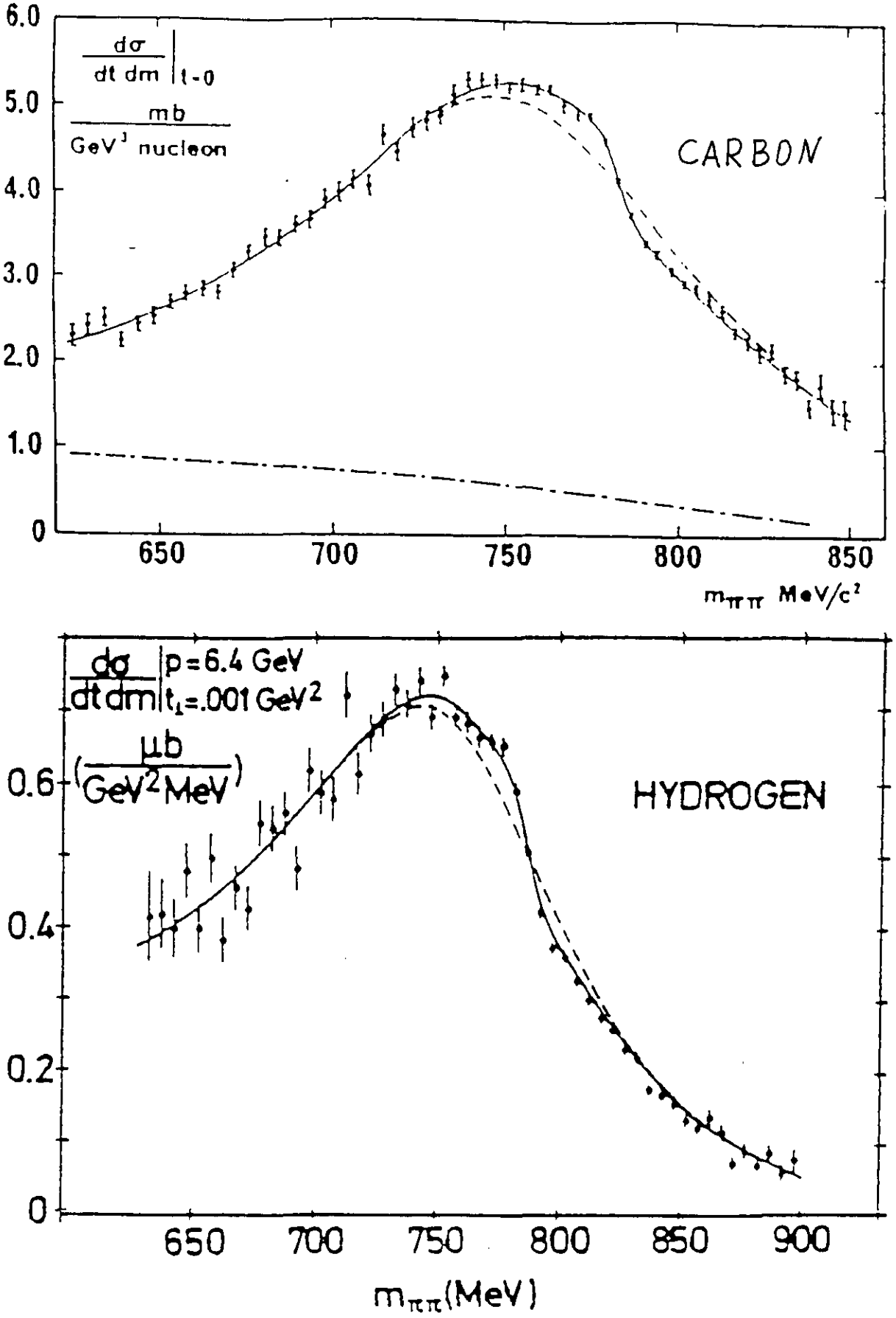

Fig.7. Effect of $\rho\omega$ mixing in $(\pi^+\pi^-)$ electroproduction

(1a,2b,3a,4b,5a,6c,7a - Tab.2) it is possible to separate M^*N^* production from M^*N reactions. This information can be used to estimate the background when one of the pions of N^* decay is interpreted as a product of the M^* decay.

Table 2. Reactions under investigation.

1. $ep \rightarrow e'\pi^+\pi^-(p)/e'\pi^+p(\pi^-)/e'\pi^-p(\pi^+)$
$f_0(\pi\pi - 78\%), f_2(\pi\pi - 85\%), f_0'(\pi\pi - 93\%), \rho_3(\pi\pi - 24\%)$
$\rho(\pi\pi - 100\%), \omega(\pi\pi - 2\%), \rho_1(\pi\pi - seen)$

2. $ep \rightarrow e'\pi^+\pi^-p(\gamma, \pi^0, \eta)/e'\pi^+\pi^+\pi^-(n)$
$\omega(\pi^+\pi^-\pi^0 - 89\%), \eta(\pi^+\pi^-\pi^0 - 24\%), \eta(\pi^+\pi^-\gamma - 5\%), \eta'(\pi^+\pi^-\eta - 44\%)$
$\rho(\pi^+\pi^-\gamma - 30\%), \phi(\rho\pi - 13\%), \phi(\pi^+\pi^-\pi^0 - 2.4\%), h_1(\rho\pi - seen)$
$b_1(\pi^+\pi^-\eta - seen), a_1(\rho\pi - 100\%), f_1(\pi^+\pi^-\eta - 13\%), a_2(\rho\pi - 70\%)$
$\omega_1(\rho\pi - seen), \omega_3(\rho\pi - seen), \pi_2(f_2\pi^0 - 56\%), \pi_2(\rho\pi - 31\%)$

3. $ep \rightarrow e'2\pi^+2\pi^-(p)/e'2\pi^+\pi^-p(\pi^-)/e'2\pi^-\pi^+p(\pi^+)$
$f_2(2\pi^+2\pi^- - 3\%), f_1(4\pi - 38\%), \rho_1(4\pi - 100\%), \rho_3(4\pi - 24\%)$

4. $ep \rightarrow e'2\pi^+2\pi^-p(\pi^0, \eta)/e'3\pi^+2\pi^-(n)$
$a_2(\omega\pi\pi - 11\%), \omega_1(\omega\pi\pi - seen), \omega_3(\omega\pi\pi - seen)$

5. $ep \rightarrow e'K^+K^-(p)/e'K^+p(K^-)/e'K^-p(K^+)$
$f_0(K\bar{K} - 22\%), a_0(K\bar{K} - seen), \phi(K\bar{K} - 49\%), \phi_3(K\bar{K} - seen)$
$f_0'(K\bar{K} - 7\%), f_2'(K\bar{K} - 71\%), \phi'(K\bar{K} - seen), a_2(K\bar{K} - 5\%), \rho_3(K\bar{K} - 2\%)$

6. $ep \rightarrow e'K^+K^-p(\pi^0/e'K^+\pi^-p(K^0)/e'K^+K^-\pi^+(n)$
$f_1(K\bar{K}\pi - 12\%), f_1'(K\bar{K}\pi - 100\%), \rho_3(K\bar{K}\pi - 4\%)$

7. $ep \rightarrow e'K^+K^-\pi^+\pi^-(p)/e'K^+K^-\pi^\pm p(\pi^\mp)/e'\pi^-\pi^+K^\pm p(K^\mp)$
$\pi_2(2K2\pi - 4\%), \phi'(2K2\pi - dominant), \phi_3(2K2\pi - seen)$

A typical example for the missing mass technique [5] is presented in Fig.8. In Fig.8a, it is shown how π^o's can be identified. The distribution in missing mass squared for E_γ=2.8 GeV is similar to the expected distribution of the events detected by CLAS, but the resolution of the CLAS detector is expected to be an order of magnitude better ($\sigma_{MMS}^{CLAS} = 0.0025GeV^2$ instead of $\sigma_{MMS}^{LBL-SLAC} = 0.025GeV^2$). In Fig.8b, one can see the identification of the ω meson. In the CLAS experiment it will be possible to achieve a statistical accuracy which is an order of magnitude higher than the previous experiments [5]. In addition the effective ω mass resolution of the CLAS detector is expected to be four times better ($\sigma_\omega^{CLAS} = 4MeV$ instead of $\sigma_\omega^{LBL-SLAC} = 17MeV$).

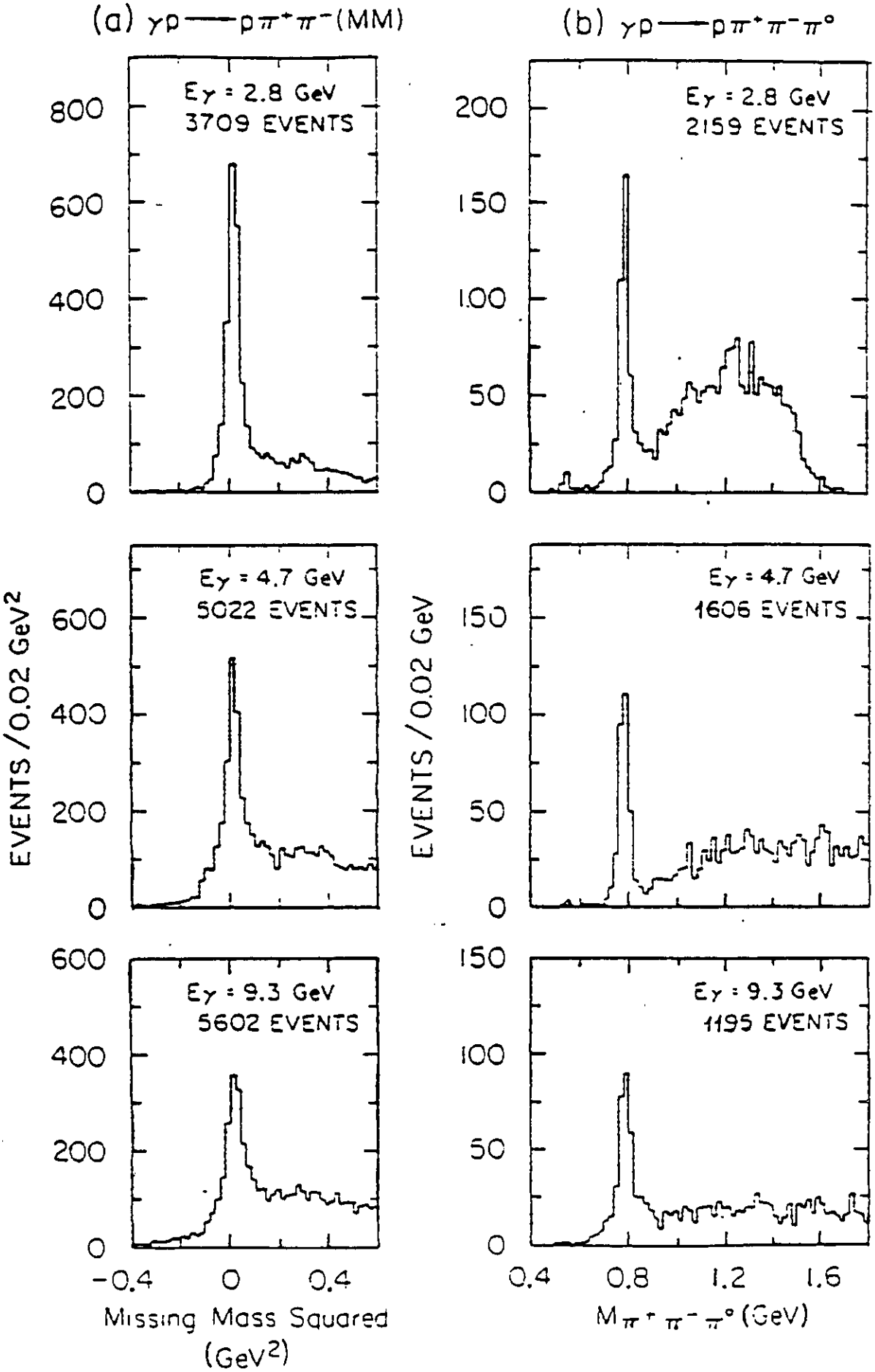

Fig.8. Missing mass reconstruction of π^0 and ω mesons

In [36] it was shown that coherent photoproduction of vector mesons on deuterium can proceed only via I=0 exchange; this can help to separate heavy resonances with large decay multiplicity from light meson production together with the baryon resonance production. So the meson production in the reaction $ed \to e'dM^*$ may be necessary to isolate the heavy vector mesons. On the other hand, the investigation of the $ed \to e'ppM^*$ reaction gives information about negative meson production. This is significant for the direct measurements of the transition form factor for ρ mesons because, in the neutral channel, the dominating diffractive contribution has to be subtracted.

3.2. Experimental Procedure for the Vector Meson Production

The proposed experiment will use the CEBAF Large Acceptance Spectrometer to measure meson electroproduction from proton and deuteron targets. The main goal of the experiment is to measure differential cross sections for the production of $q\bar{q}$ states as a function of Q^2. The high efficiency of the CLAS detector will allow to identify mesons not only by the missing mass in the $ep \to e'pX$ reaction but also via the analysis of the angular distributions of the decay products. This is necessary for the investigation of the meson decay angle correlations.

The data acquisition system should be triggered by the detection of the scattered electron, thus giving an unbiased data sample for the hadronic final state. A typical ω electroproduction event at 4 GeV is sown in Fig.9. The ϕ distribution of the secondary particles is shown in the small hexagonal graph and two triples of the combined sectors are shown as a middle plane projections. The first constraint for the efficiency is the electron acceptance of the detector. We estimated it roughly when we considered the kinematical region under investigation. The efficiency distribution in the kinematical regions is shown in Fig.10-15. In Fig.10 the acceptance for a 2 GeV energy beam (half field) is shown. Events were accepted in the histogram shown in Fig.10a under the following conditions:

- (i) the electron was detected by all 6 drift chambers, by TOF scintillator counters, by Cherenkov counters and by the electromagnetic calorimeter,
- (ii) at least 3 more hadrons have been detected,
- (iii) the positive hadron is detected by all 6 drift chambers and by TOF scintillator counters,
- (iv) the negative pion is detected by all 6 drift chambers,
- (v) the neutral pion is accepted if both gammas are detected by the electromagnetic calorimeter.

A special group of events are those that have 4 detected particles in the final state including a neutral pion. For this type of event the angular resolution for the 3π decay in the ω C.M.S. is worse than for where all charged particles are detected because the angular and momentum resolutions for π^0 is worse than for charged

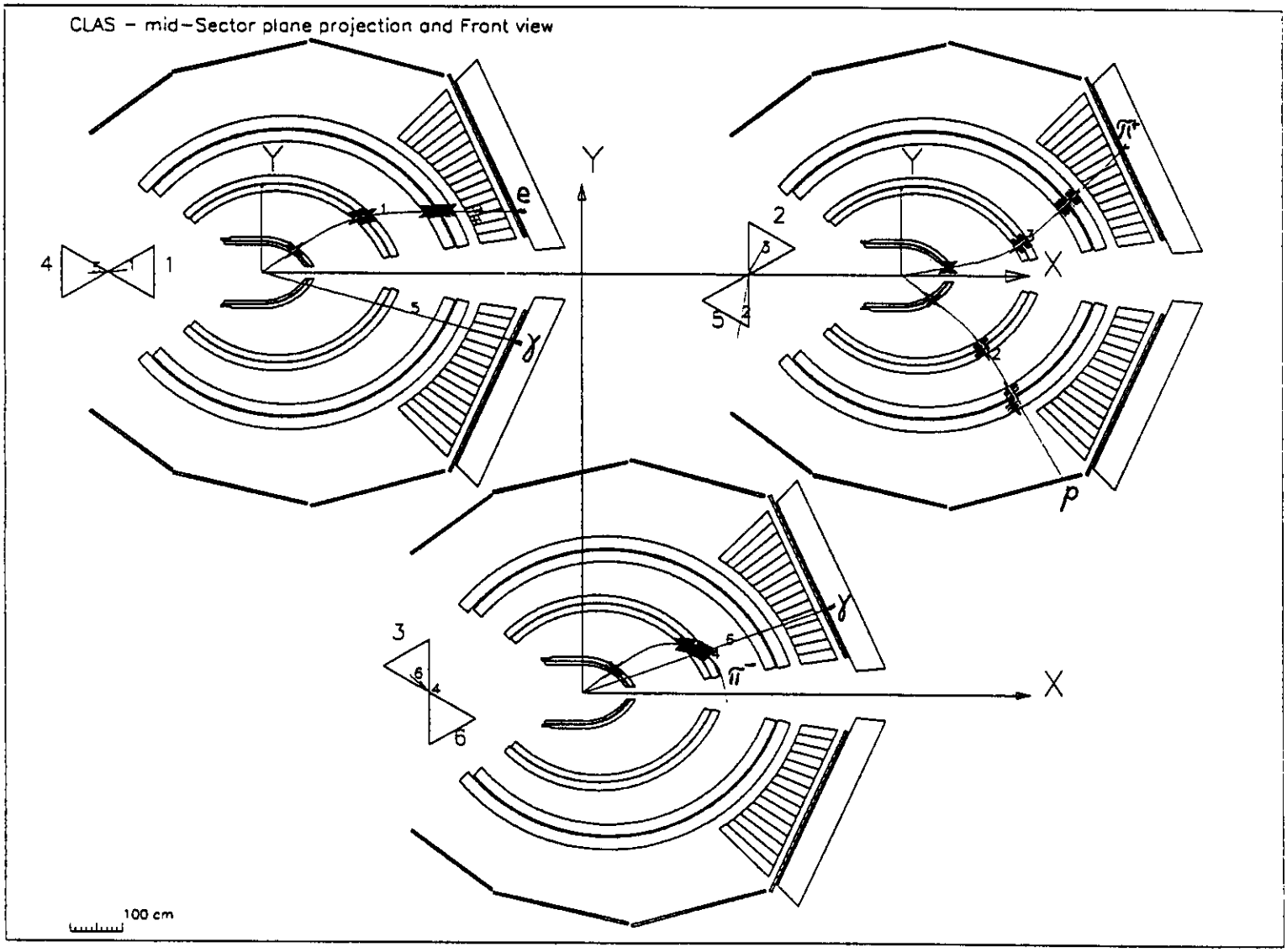

Fig.9. Electroproduction of ω meson in CLAS detector

Fig.10. CLAS efficiency for ω electroproduction at E=2 GeV (half field)

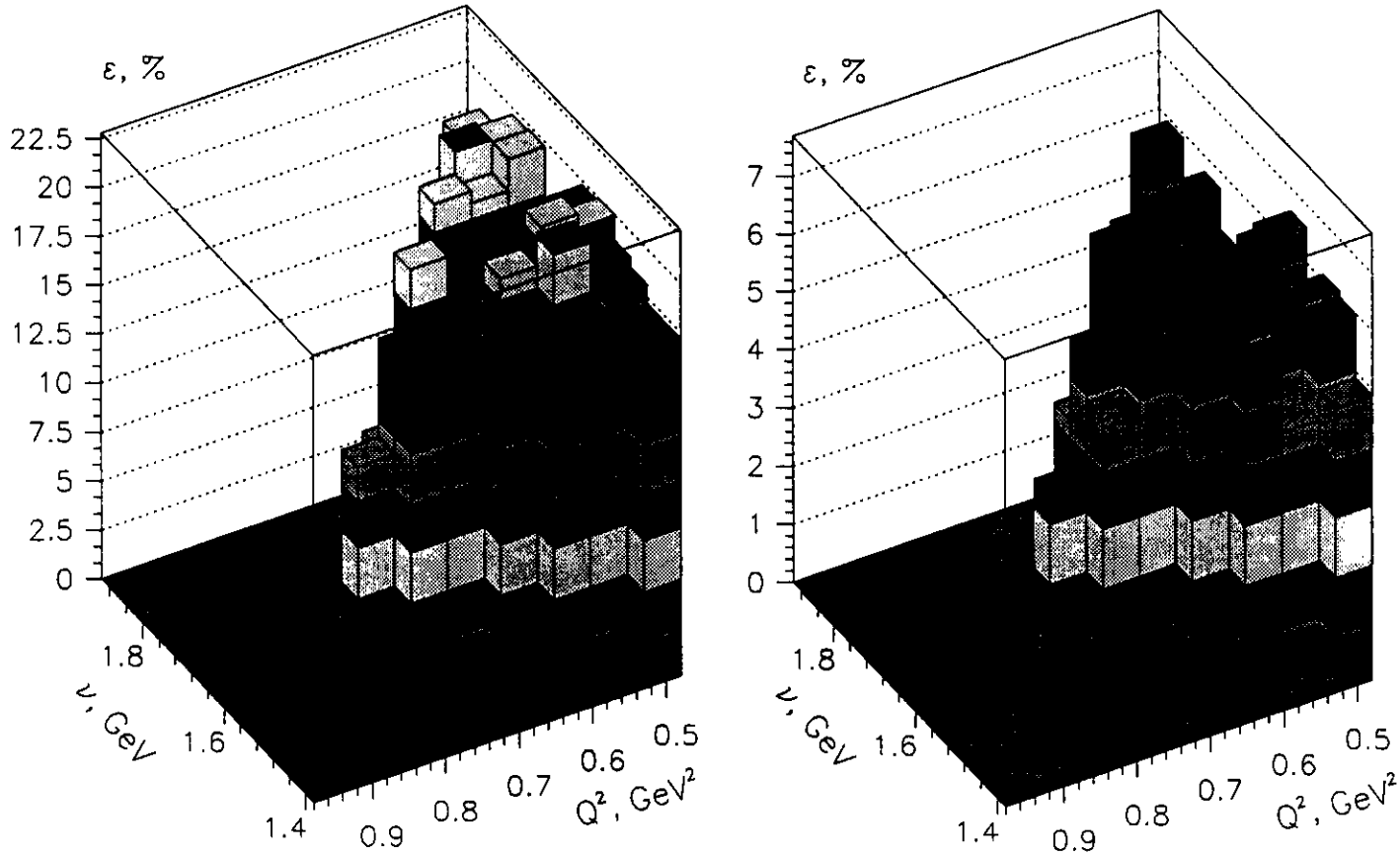

(a) Efficiency for 5 and 4 (including e)

(b) Efficiency for e + π^0 + 2 hadrons

particles. Therefore, this part of the acceptance is shown separately in Fig.10b. One can see that for a 2 GeV energy beam one third of the detected events will include a detected π^0. The efficiency for a beam energy 2 GeV and for the same conditions have been calculated for the full field (Fig.11). One can see that for the full field the efficiency is lower by a factor of two. Therefore half of magnetic field should be used at 2 GeV. For a 3 GeV energy beam the efficiency for full and half magnetic field is approximately the same(Fig.12). In this case because of the better resolution the full field is preferable.

For a 4 GeV energy beam events with detected π^0 correspond to 2/3 of the total efficiency (Fig.13) because the ω energy meson increases and angular decay cone of the π^0 becomes narrower. In Fig.13a the efficiency for 4 detected particles including π^- is shown. Because of the small acceptance for π^- this efficiency is approximately equal to the efficiency for all 5 detected particles including π^0 (Fig.14b). For a 6 GeV energy beam the efficiency is even slightly higher then for 4 GeV (Fig.15), but the percentage of events with detected π^0 is approximately the same.

3.3. Cross Section Calculation

For the description of the cross section, we fixed the diffractive part without a longitudinal contribution and added the one-pion exchange contribution to describe ω production. The description of the Q^2 dependence of the $\frac{\sigma_\omega}{\sigma_\rho}$ ratio is shown in Fig.16. The constant 1/9 corresponds to the contribution of the diffractive mechanism to the ω electroproduction. One can see that, at the present level of the experimental accuracy, the description is rather good. Hence, as the ρ meson production is described by the model (Fig.5), the simulation of the ω production must be reliable too.

The experimental data of [4] and [5] for the ω photoproduction are shown in Fig.17. One can see that the model describes the experimental data except for low photon energies (E_γ=1.6 GeV, W=2.17 GeV) and large momenta transferred to proton($-t > m_\omega^2$). One possible explanation of the enhancement is the production of an ωN resonance with a mass around 2 GeV.

The situation is more complicated for electroproduction. The cross section for a ω-meson electroproduction was measured in one experiment, only [7]. The t dependence is shown in Fig.18. The curve in the figure demonstrates the calculations in the framework of the model described above. For low W, an additional contribution at large $-t$ ($-t > m_\omega^2$) is clearly seen. It would be interesting to check if this additional contribution will disappear at large W (as for the photoproduction), or it may be determined by the dual diagram (Fig.2e) and hence depends only slightly on W.

Fig. 11. CLAS efficiency for ω electroproduction at E=2 GeV (full field)

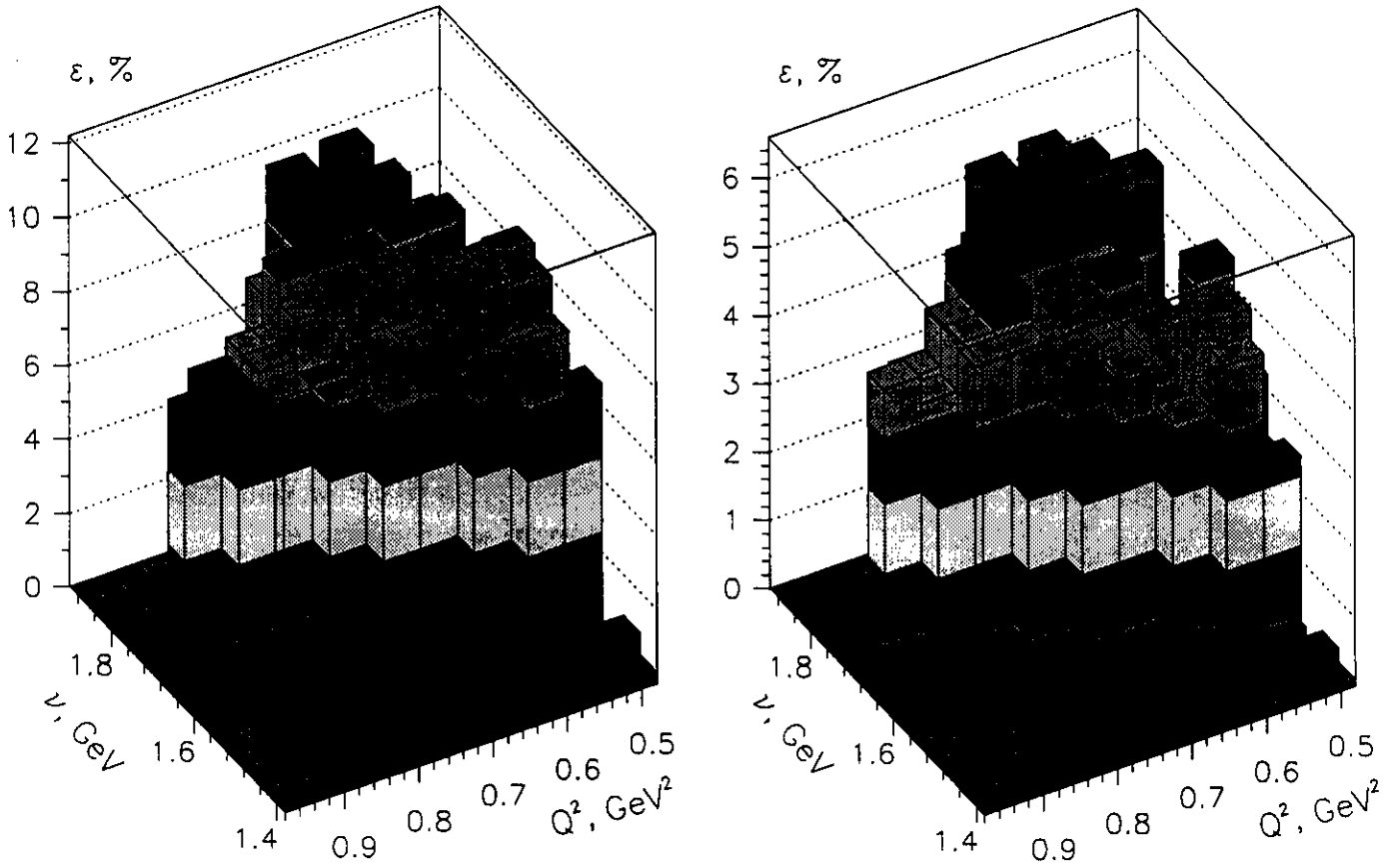

(a) Efficiency for 5 and 4 (including e)

(b) Efficiency for e + π^0 + 2 hadrons

Fig.12. CLAS efficiency for ω electroproduction at E=3 GeV

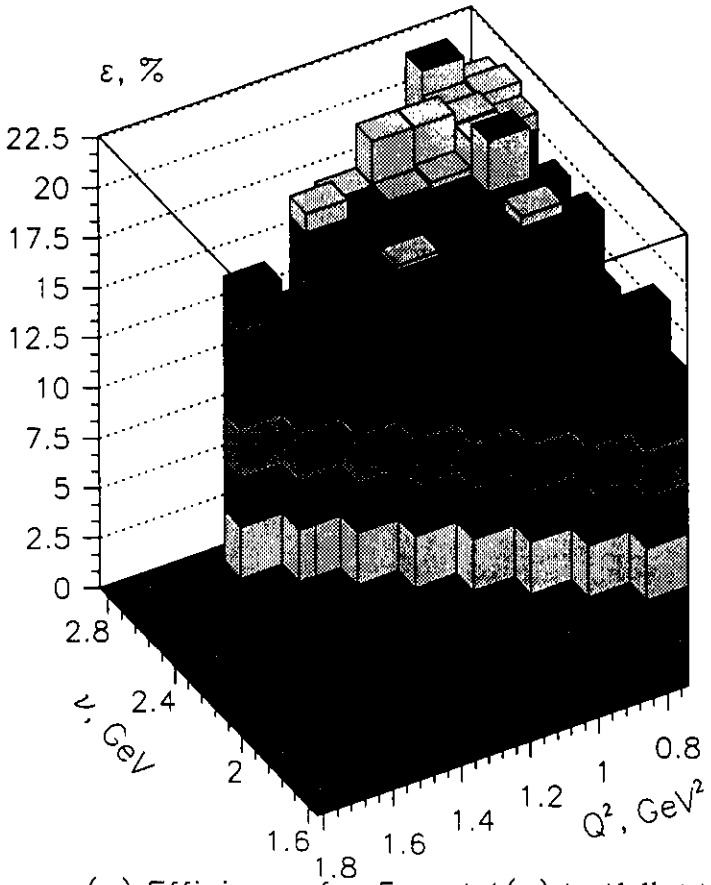

(a) Efficiency for 5 and 4(e) half field

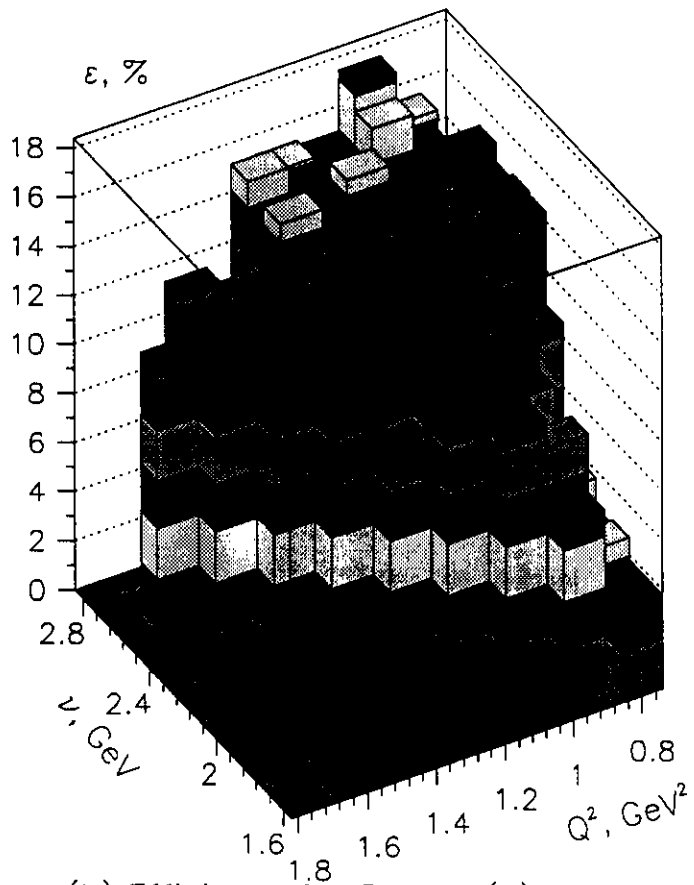

(b) Efficiency for 5 and 4(e) full field

Fig. 13. CLAS efficiency for ω electroproduction at E=4 GeV (full field)

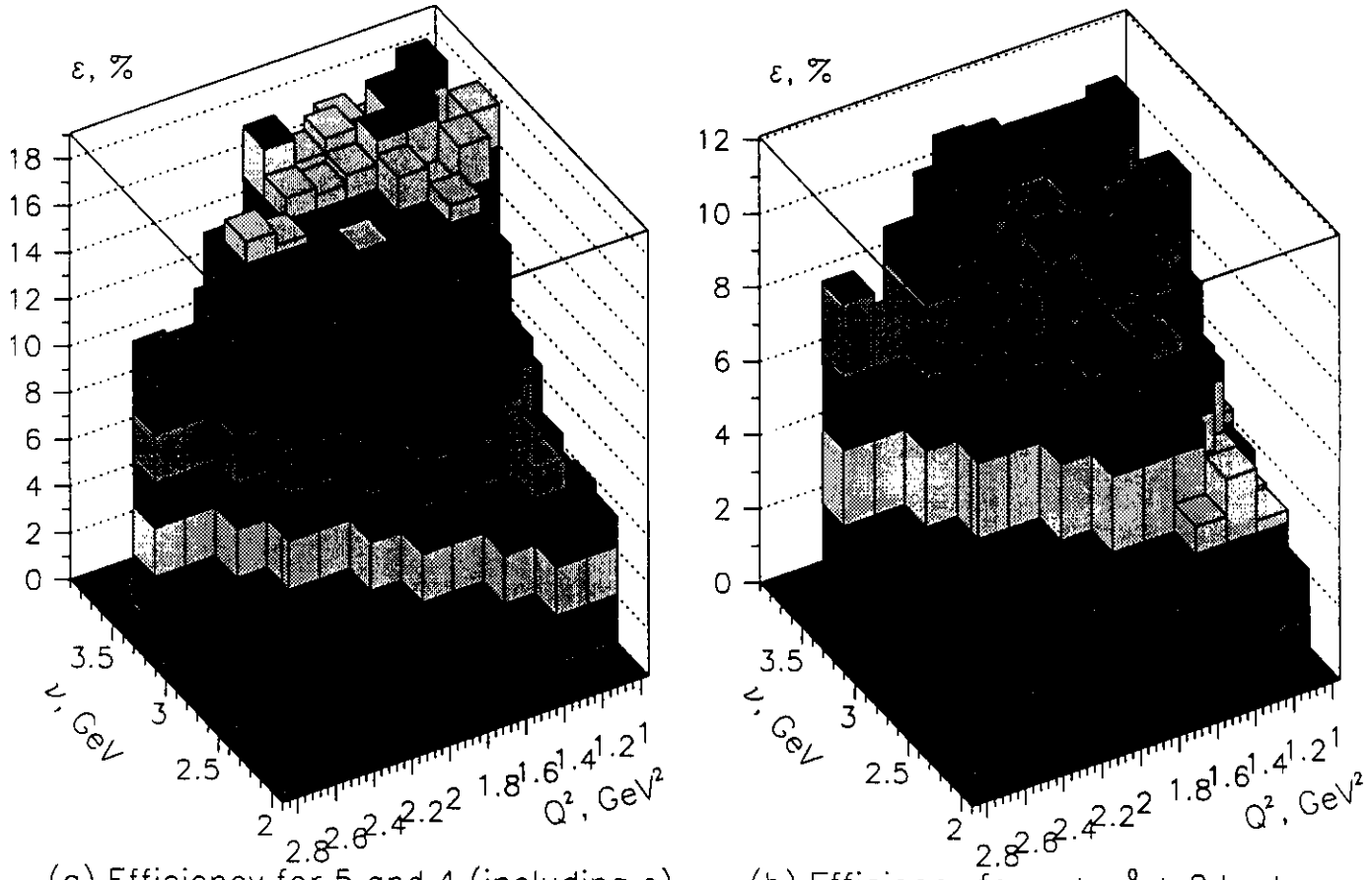

(a) Efficiency for 5 and 4 (including e)

(b) Efficiency for e + π^0 + 2 hadrons

Fig. 14. CLAS efficiency for ω electroproduction at E=4 GeV (full field)

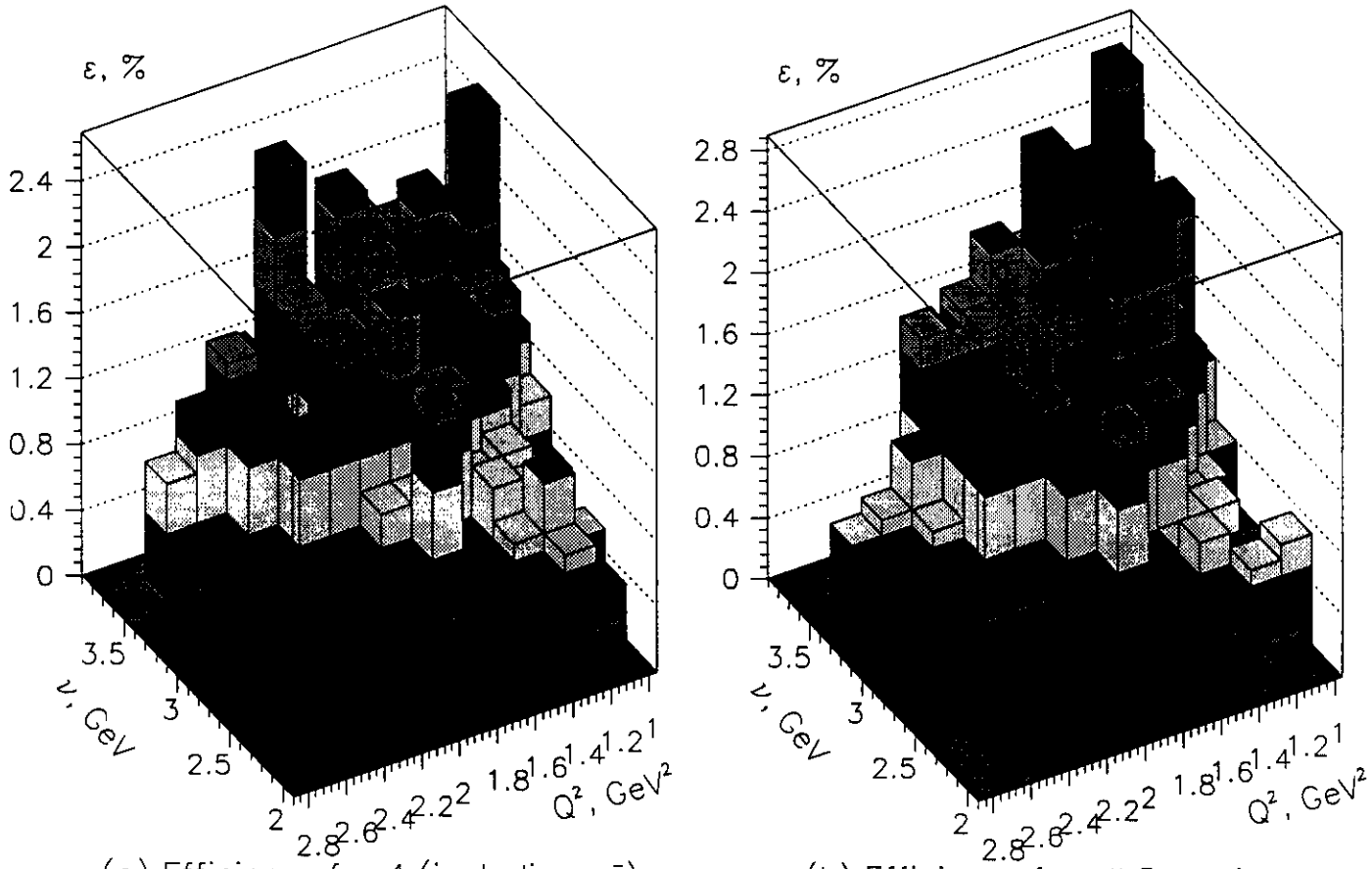

(a) Efficiency for 4 (including π^-)

(b) Efficiency for all 5 particles

Fig.15. CLAS efficiency for ω electroproduction at E=6 GeV (full field)

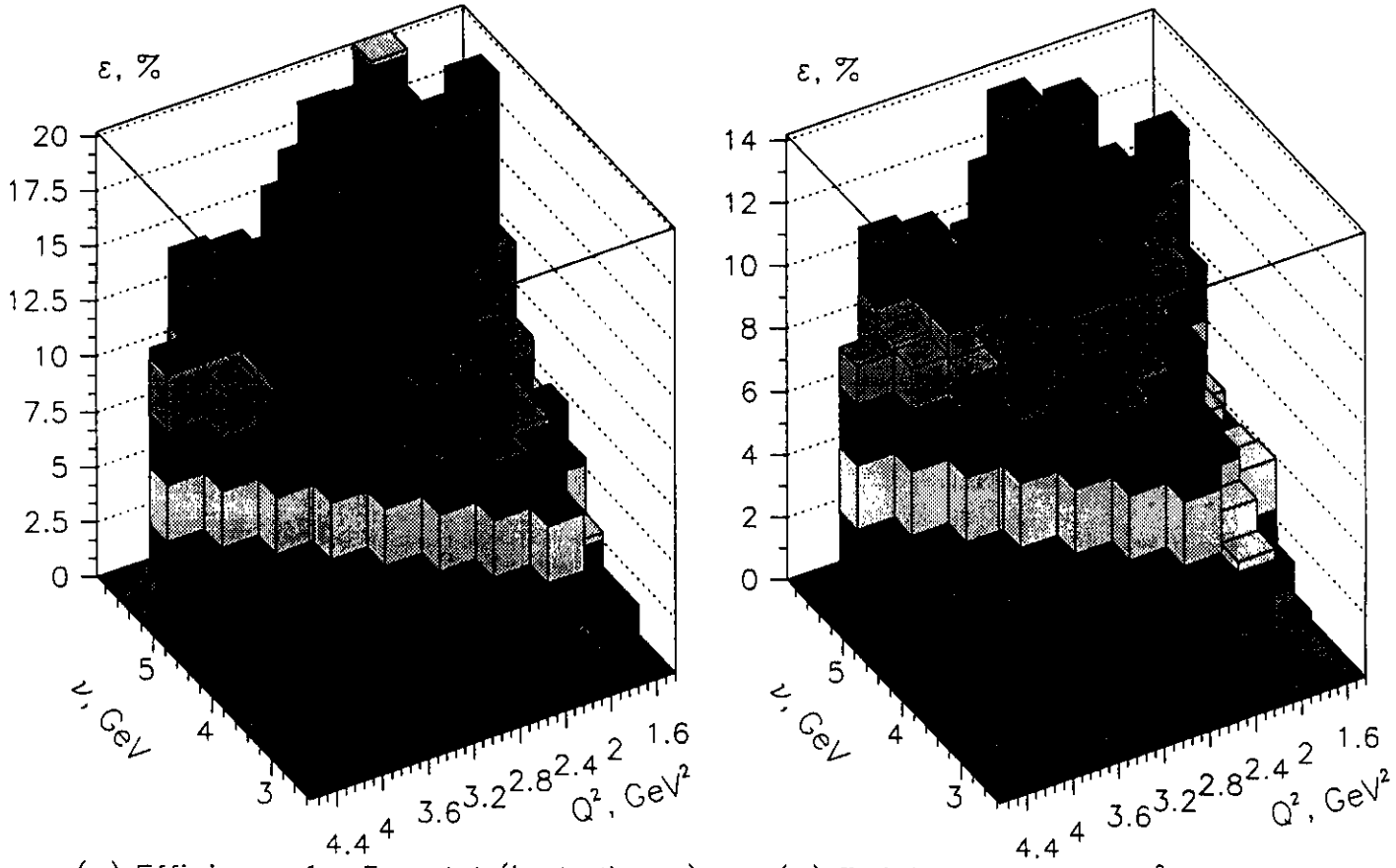

(a) Efficiency for 5 and 4 (including e)

(b) Efficiency for e + π^0 + 2 hadrons

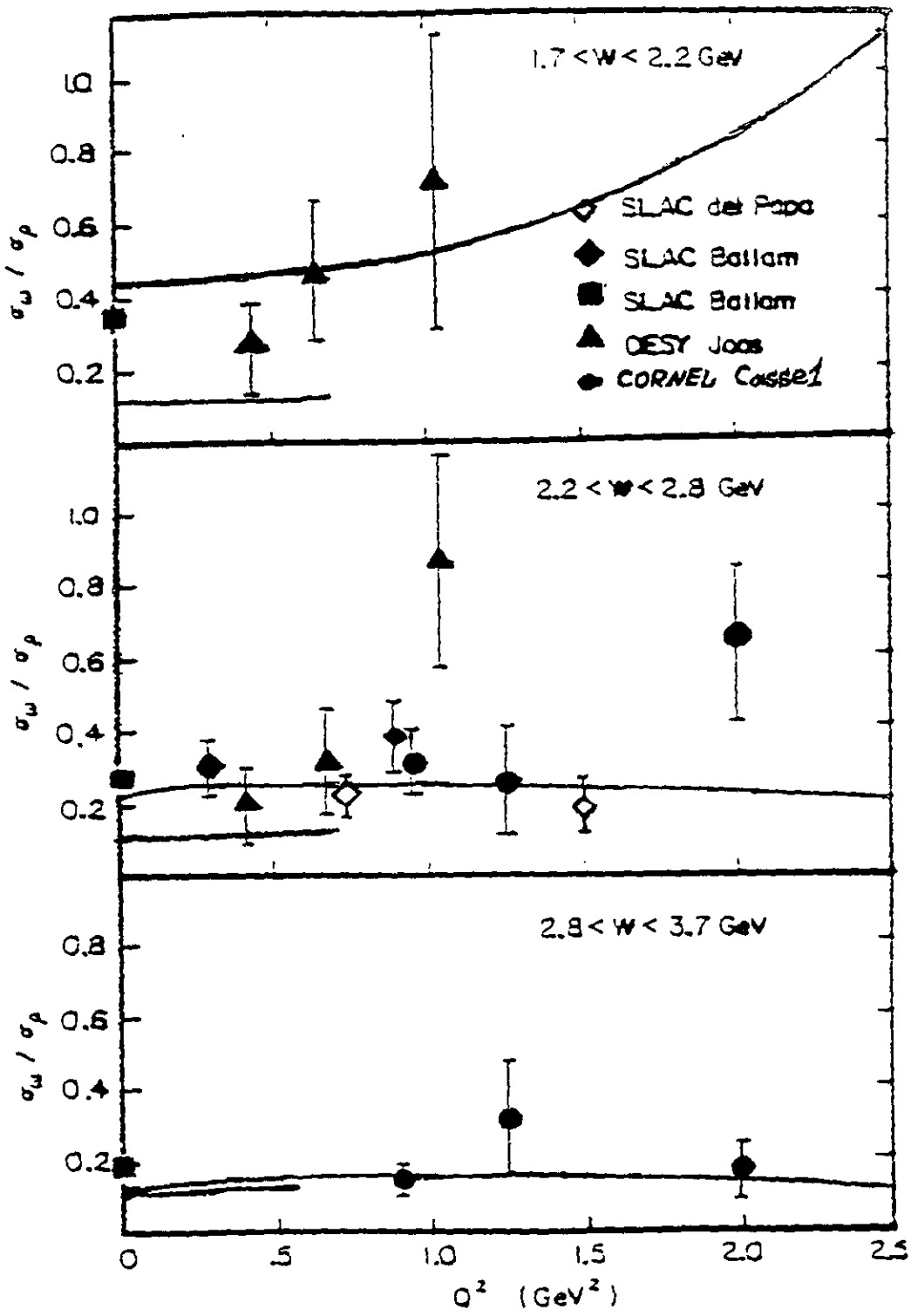

Fig. 16. Q^2 dependence of $\sigma_\omega/\sigma_\rho$ ratio

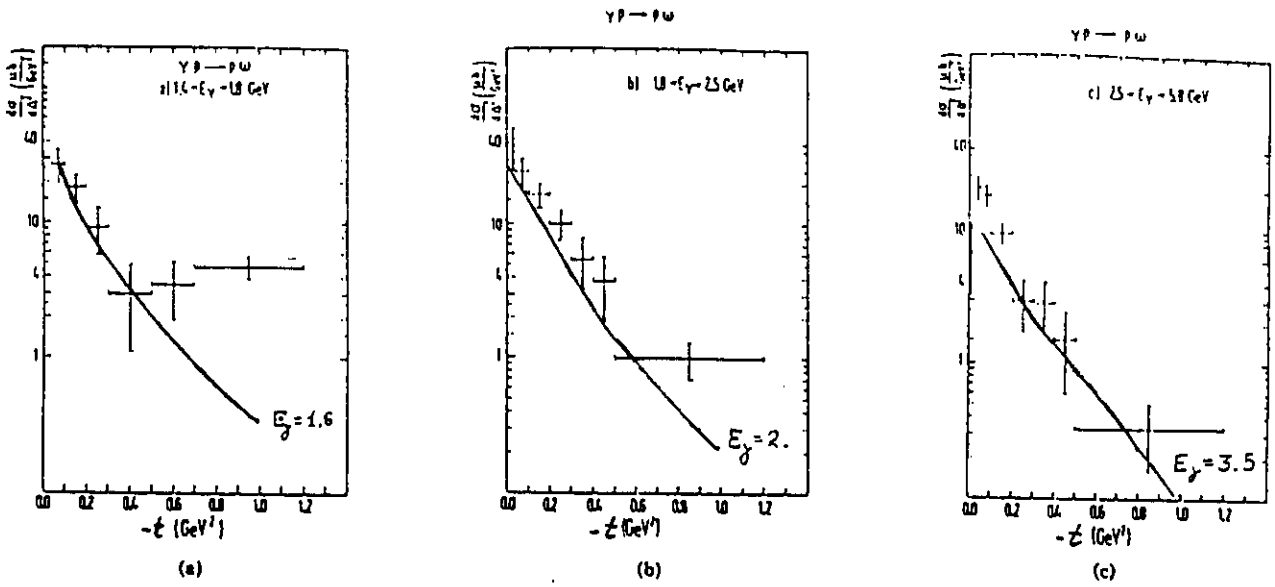

γp —— pω

LBL-SLAC J.Ballam et al. (1973)

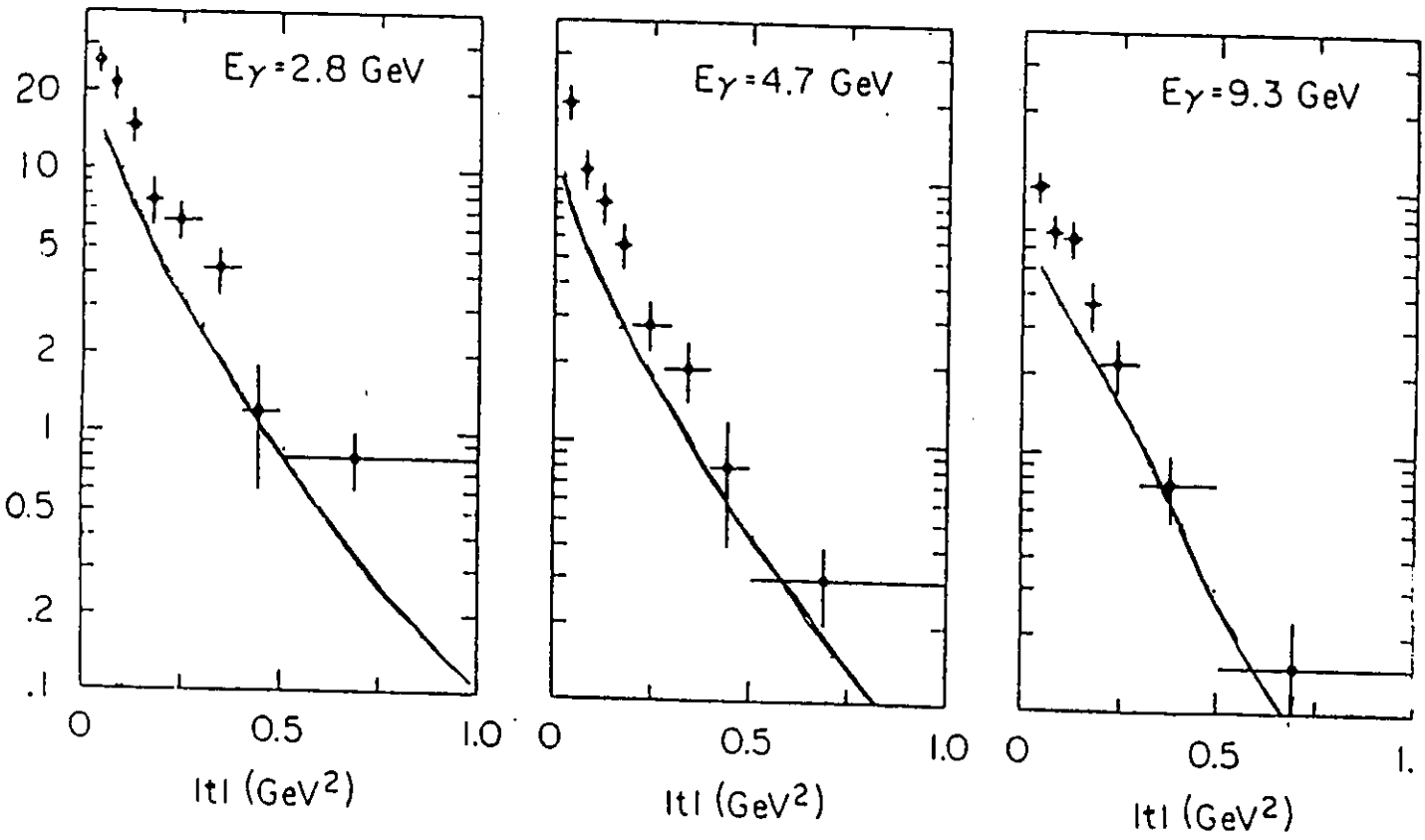

Fig. 17. t-dependence of ω photoproduction

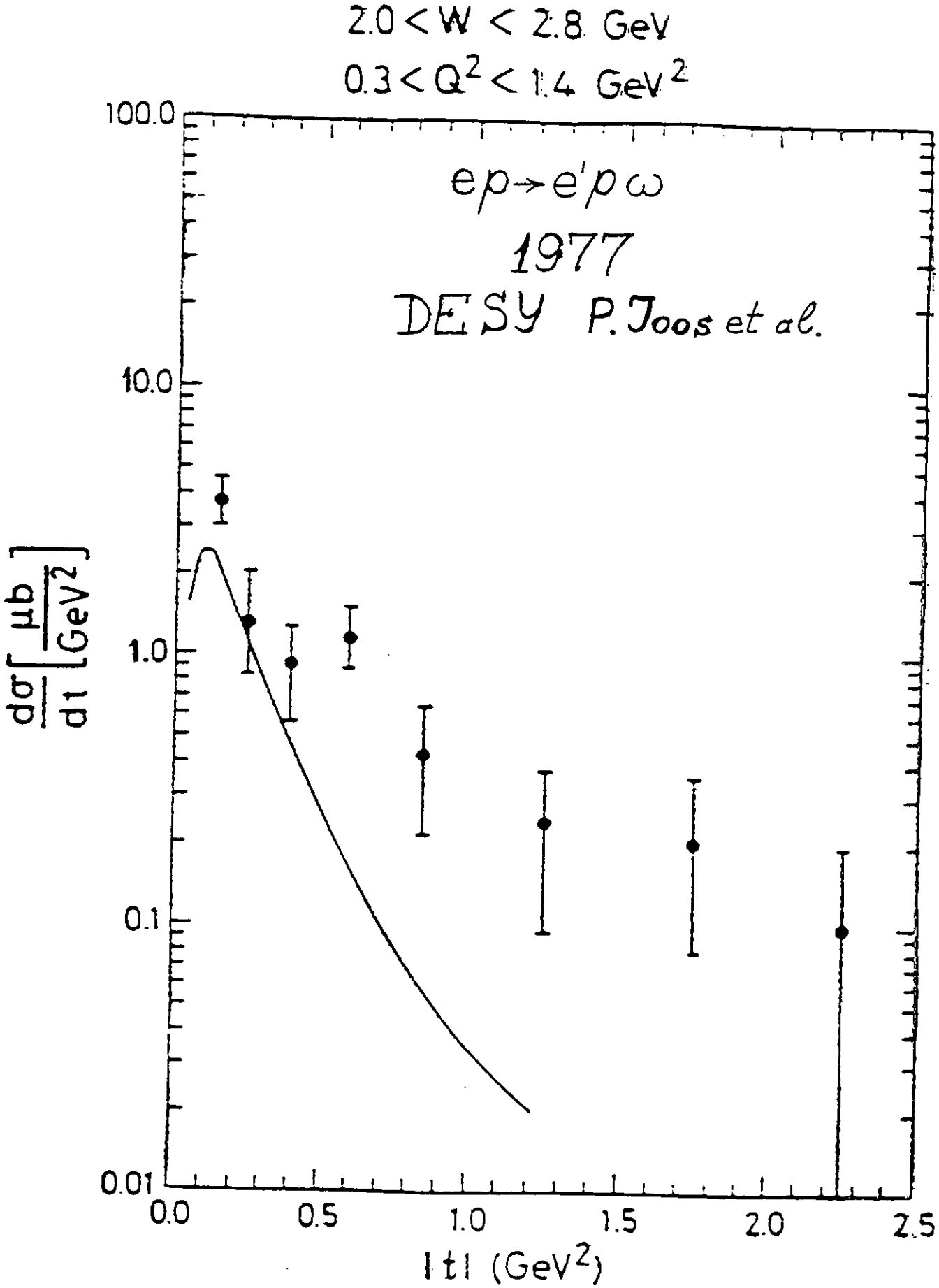

Fig. 18. t–dependence of ω electroproduction

4. Expected results

4.1. Monte Carlo Simulation of ω Electroproduction

For the simulation of the meson production events the model described in Appendix C has been used. Figures 19-21 show ν-, t- and Q^2 dependences for different primary electron energies (2, 3, 4, and 6 GeV). The transferred energy dependence is shown in Fig.19. The black points correspond to diffractive production, empty triangles to the longitudinal part of the OPE production, and empty squares to the transverse part of the OPE production. The number of events in each bin corresponds to 300 hours of beam time at a luminosity of $10^{34} cm^{-2} sec{-}1$ and an efficiency of 10%. In the figure one can see that, at low primary electron energies, the OPE mechanism dominates and can be easily separated. A large primary electron energies, diffraction dominates at least at high transferred energies.

In Fig.20 the t-dependence of the event rate calculated in the framework of the Fraas model is shown. It is clear that, at large momenta transferred to the proton, the OPE mechanism dominates. On the other hand, at large transferred momenta the s-channel resonances can contribute to the cross section of the reaction. Fortunately, the contribution of exotic resonances, which could decay to ω meson and nucleon, is expected to be large at low energies, only.

In Fig.21 the Q^2-dependence of the event rate is shown. One can see that the shape of the Q^2 dependence is similar for the diffraction and OPE mechanisms. This is a model prediction that has never been checked experimentally. But it permits to estimate of the accuracy of the expected experimental data which are necessary for the calculation of the transition form factors. For the comparison, exponential transition form-factors of the naive quark model (curves in Fig.21) have been used in the simulation instead of the Wolf [37] transition form-factors. These approximate the known experimental data and have have been used in the framework of Fraas model. One can see that at $Q^2 \leq 1$ GeV, where the naive quark model is verified, the differences between the form-factors are small. At large Q^2, relativistic corrections to the nave quark model should be taken into account [38]

4.2. An anomalous Longitudinal Polarization in ρ Electroproduction

In the CEBAF Q^2 region it is possible to measure more than half of anomalous effect of the longitudinal polarization in ρ electroproduction (Fig.6). High angular resolution and high rate of ρ-meson electroproduction permit to measure the Q^2 dependence of ρ-meson polarization with high accuracy. Polarized hydrogen target and polarized electron beam could give additional information about the anomalous spin-flip amplitude in diffractive ρ-meson electroproduction.

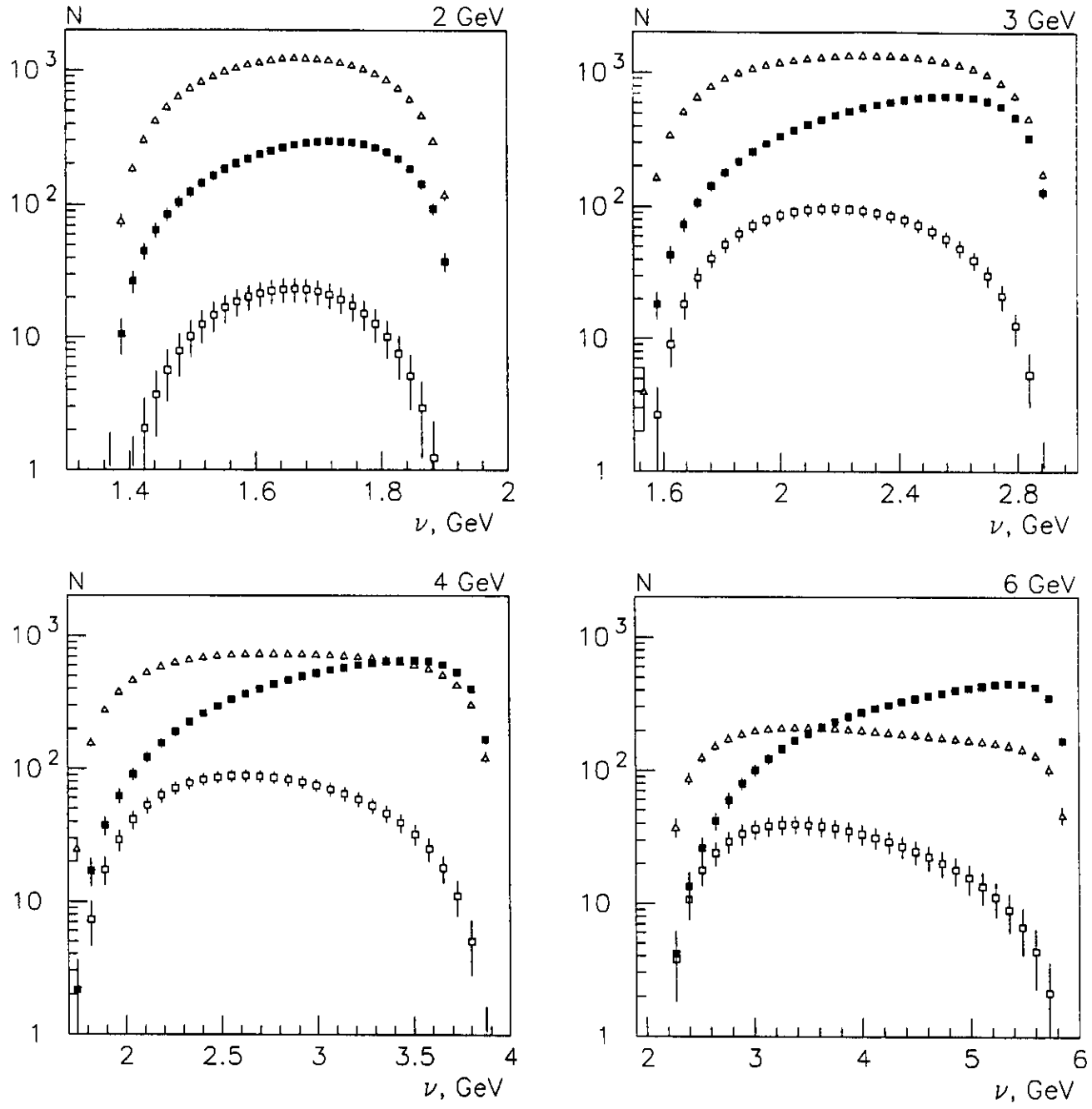

Fig.19. Simulated ν–dependence of the event rate

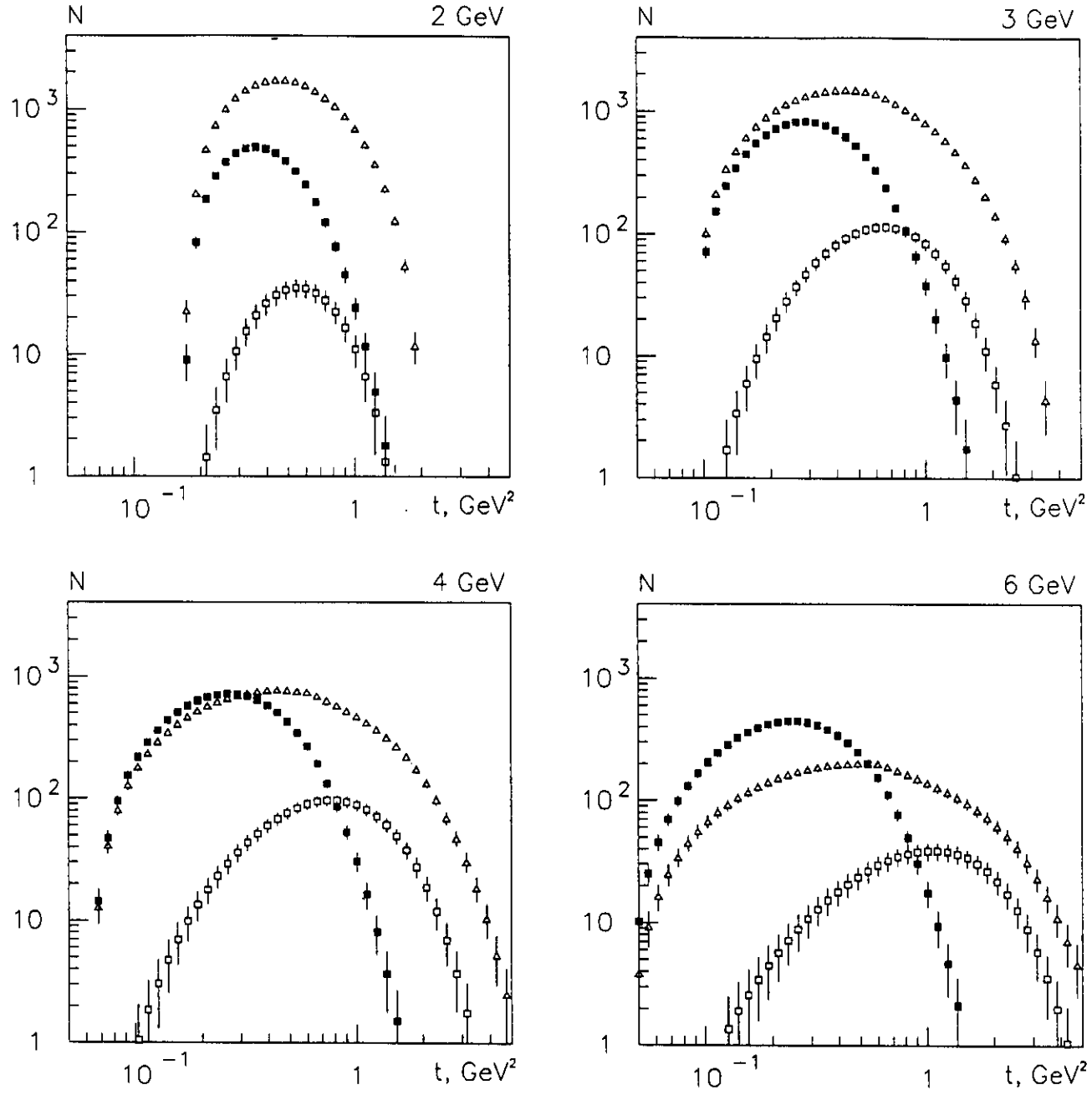

Fig.20 Simulated t−dependence of the event rate

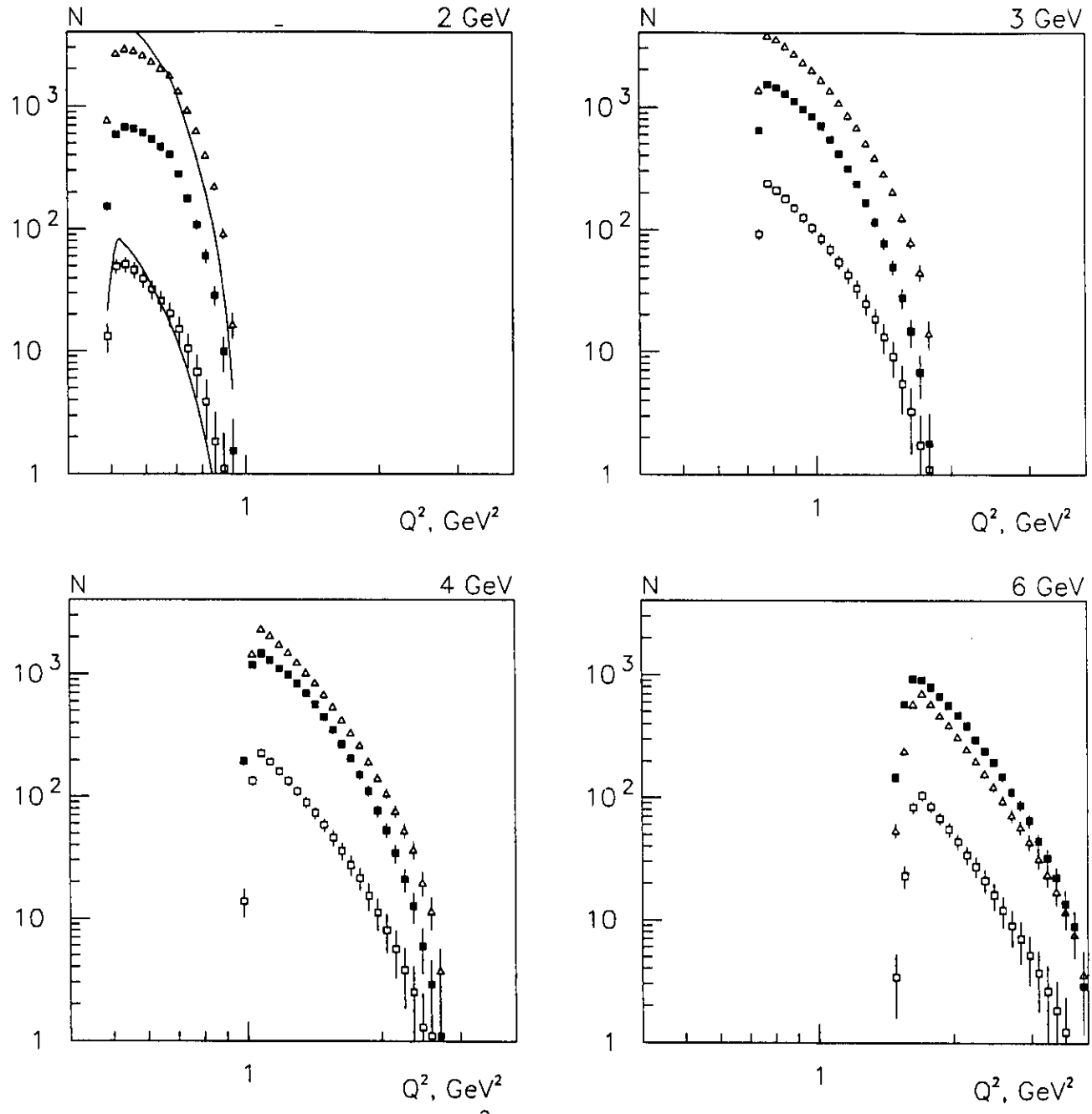

Fig.21. Simulated Q^2–dependence of the event rate

Table 1. Light Quark Mesons

Meson	Mean efficiency	2 GeV	3 GeV	4 GeV	6 GeV
ω	10%	90	130	90	40
ρ	20%	140	310	300	200

4.3. Measurement of the $\rho\omega$ Mixing Effect

At a beam energy of 4 GeV the number of events in the $\pi^+\pi^-$ mass distribution presented in Fig.7 can be collected by CLAS during 100 hours of beam time. So in the CLAS experiment, it is possible to investigate not only the $\rho\omega$ mixing but its Q^2-dependence too. Large acceptance of CLAS permits to have uniform statistical errors for all region of the $\pi^+\pi^-$ effective mass.

5. Future Developments

The main future development of the experiment is associated with the investigation of high radial excitations of $q\bar{q}$ system. The future upgrade of the CEBAF accelerator (6 GeV energy beam) will open the possibility to study the D-states of $q\bar{q}$ system, half of which have not yet been discovered. The perspective of this investigation will be made clear after the first measurements at 4 GeV which should give information about P- and 2s-states of $q\bar{q}$ system.

The other direction of the development is an investigation of the electroproduction of vector mesons on nuclear targets. Because of the high efficiency for the detection of π^0 it is possible to detect not only ρ mesons via their π^+, π^- decay mode but ω mesons by π^+, π^-, π^0 decay mode, too. The vector meson electroproduction permits an analysis of pionic degrees of freedom in nuclei, secondary interactions of ω mesons with nuclei (ωN resonances), and effect of color transparency for meson states.

Finally, for the complete analysis of Q^2-dependence of the meson electroproduction a number of Q^2=0 (tagged photons) measurements may be needed.

6. Count Rate Estimates and Run Time Request

The following assumptions were used in estimating the ω and ρ count rate due to resonance formation:

(i) Luminosity: $L = 10^{34} cm^{-2} sec^{-1}$,

(ii) CLAS average efficiency for the detection of $e'p\pi^+\pi^-$ final state particles = 0.1

(iii) CLAS average efficiency for the detection of three charged particles in the final state (ρ meson) = 0.2.

Appendix A Observables and Response Functions

The kinematics for pion electroproduction are illustrated in Fig. 17. The angle between the leptonic scattering plane (containing the initial and final electron 3-vectors) and the hadronic reaction plane (containing the 3-momentum transfer q and the final nucleon 3-momentum $\mathbf{p}_{N_f}$) is denoted by $\phi_N = \phi_\pi - 180°$. The angles between the 3-momentum transfer and the laboratory momenta of final nucleon momentum and the pion are denoted by θ_N and θ_π, respectively. Note that for $\phi_N = 0°$ and $\theta_N > 0°$, the nucleon recoils at a more forward angle than the 3-momentum transfer. The hadronic center of momentum frame is defined by the condition $\mathbf{q}^* + \mathbf{p}^*_{N_i} = \mathbf{p}^*_{N_f} + \mathbf{p}^*_\pi = 0$. The response functions can be considered functions of the invariant quantities

$$Q^2 = -q^2 = -(k_i - k_f)^2 = 2k_i k_f \sin^2(\theta_e/2)$$

$$W = \sqrt{s} = \sqrt{(q^* + p^*_{N_i})^2} = \sqrt{(p^*_\pi + p^*_{N_f})^2} = E^*_\pi + E^*_{N_f}$$

and the c. m. recoil nucleon angle $\theta^*_N = 180° - \theta^*_\pi$.

The recoil polarization is usually measured with respect to the helicity frame defined by the basis vectors

$$\begin{aligned} \hat{\mathbf{l}} &= \frac{\mathbf{p}^*_N}{|\mathbf{p}^*_N|} \\ \hat{\mathbf{n}} &= \frac{\mathbf{q}^* \times \hat{\mathbf{l}}}{|\mathbf{q}^* \times \hat{\mathbf{l}}|} \\ \hat{\mathbf{t}} &= \hat{\mathbf{n}} \times \hat{\mathbf{l}}. \end{aligned}$$

This basis is well defined when θ^*_N is not equal to 0° or 180°, but difficulties arise when $\mathbf{q}^*$ and $\mathbf{p}^*_N$ are either parallel or antiparallel and ϕ_N loses physical meaning. These cases are conventionally handled by first rotating the reaction plane to $\tilde{\phi}_N$ as it would be in non-parallel kinematics, and then taking the limit $\theta^*_N \to 0°$ or $\theta^*_N \to 180°$ as required.

The electroproduction cross section can be expressed in the form

$$\frac{d\sigma}{d\omega d\Omega_e d\Omega^*_N} = \frac{1}{2}\sigma_0 \left[1 + \vec{P} \cdot \vec{\sigma} + h(A + \vec{P}' \cdot \vec{\sigma})\right] \qquad \text{(A.1)}$$

where $\sigma_0 = K\tilde{\sigma}_0$ is the unpolarized cross section, $\vec{P}$ is the induced-polarization coefficient, A is the beam analyzing power, $\vec{P}'$ is the polarization-transfer coefficient, h is the electron helicity, and $\vec{\sigma}$ is the nucleon polarization vector. Thus, the net polarization of the recoil nucleon $\vec{\Pi}$ has two contributions of the form

$$\vec{\Pi} = \vec{P} + h\vec{P}'. \qquad \text{(A.2)}$$

Appendix A: Diffractive and OPE contributions to M* production.

It is possible to calculate the relative contribution of the diffractive and OPE mechanisms in isoscalar and isovector meson production by analyzing the Lagrangians for the $\pi\gamma M^*$ and $P\gamma M^*$ interactions (P means Pomeron exchange and symbolizes the diffractive process). The general form for the Lagrangians is:

$$L = e_u\bar{u}\gamma^\mu u + e_d\bar{d}\gamma^{mu}d,$$

where e_u is the charge of the u-quark, and e_d is the charge of the d-quark. It can be rewritten as a superposition of the I=1 and I=0 terms:

$$L = \frac{e_u - e_d}{2}(\bar{u}\gamma^\mu u - \bar{d}\gamma^\mu d) + \frac{e_u + e_d}{2}(\bar{u}\gamma^\mu u + \bar{d}\gamma^\mu d)$$

The charge $\frac{e_u-e_d}{2} = \frac{1}{2}$ is three times larger than the charge $\frac{e_u+e_d}{2} = \frac{1}{6}$, and hence the contribution of the first term is nine times larger than the contribution of the second one.

For the $\rho\pi\gamma$ vertex ($I_\rho = 1$ and $I_\pi = 1$), only the isoscalar part (second term) of the Lagrangian describes the vertex. In the case of the $\omega\pi\gamma$ vertex ($I_\omega = 0$ and $I_\pi = 1$), only the isovector part (first term) should be taken into account. In analogy, one should take the isoscalar part of the $\rho P\gamma$ vertex ($I_\rho = 1$ and $I_P = 0$) and the isovector part of the $\omega P\gamma$ vertex ($I_\omega = 0$ and $I_P = 0$). This simple consideration leads to the conclusion that the contribution of the diffraction to the production of the isovector mesons is nine times larger than the diffractive contribution to the production of the isoscalar mesons and, on the contrary, the OPE contribution to the production of isovector mesons is nine times less than the OPE contribution to the production of isoscalar mesons.

The other possibility to estimate the same relative contributions is a VMD method. Let us consider the photon as a superposition of ρ and ω mesons. It is known from the experiment that the $\gamma\omega$ coupling constant ($\frac{f_\omega^2}{4\pi} = 18.4$) is nine times larger then the $\gamma\rho$ coupling constant ($\frac{f_\rho^2}{4\pi} = 2.18$) [39]. For the diffraction this ratio of coupling constants defines the relative contributions of ω and ρ mesons. The OPE mechanism transforms ω into ρ and ρ into ω, so the ratio should be reversed.

Appendix B: Kinematics of the ep→e'pM* reaction.

Let $(\nu, \bar{q})$ be the 4-momentum of the virtual photon and $(\sqrt{p^2+m_p^2}-m_p, \bar{p})$ be the 4-momentum transferred to the proton (m_p is a mass of the proton). Then the threshold condition for M^* production is $W^2=(\nu+m_p)^2-q^2 \geq (m_p+M)^2$, where M is a mass of the M^* meson. To obtain the minimum momentum transfer one can write the equation: $(\nu+m_p-\sqrt{m_p^2+p^2})^2-q^2-p^2+2pq=M^2$. The solution of this equation is

$$p_{min}=\frac{q(\nu^2-M^2+m_p^2)-(\nu+m_p)\sqrt{(W^2-M^2-m_p^2)^2-4M^2m_p^2}}{2W^2}.$$

Then, the minimal $-t$ can be found as $-t_{min}=2m_p(\sqrt{p_{min}^2+m_p^2}-m_p)$.

The diffractive and OPE mechanisms for M^*-production dominate when $-t < M^2$. The condition $-t=M^2$, $cos(\theta_{pq})=1$ may be written as follows: $(\nu+\frac{t}{2m_p})^2-(p-q)^2=M^2$. To define the $Q^2=Q^2_{max}(\nu)$ dependence one can use the equation $Q^4+2Q^2\frac{M^2}{m_p}(\nu-\frac{M^2}{2m_p})+4M^2(\frac{\nu M^2}{m_p}+M^2-\nu^2)=0$. It may be solved under the threshold condition $\nu \geq \frac{M}{m_p}(M+\sqrt{M^2+m_p^2})$. The solution of this equation is

$$Q^2_{max}(\nu)=M\sqrt{(4+\frac{M^2}{m_p^2})[(\nu-\frac{M^2}{2m_p})^2-M^2]}-\frac{M^2}{m_p}(\nu-\frac{M^2}{2m_p}).$$

To know $(-t_{min})$ and $(-t_{max})$ for given values of W and Q^2 one should know the initial (p_1) and final (p_2) momenta of the proton in the rest frame of the $\gamma p \rightarrow pM^*$ reaction. The momenta can be calculated as $p_1=\sqrt{(W^2+Q^2-m_p^2)^2+4Q^2m_p^2}/2W$ and $p_2=\sqrt{(W^2-M^2-m_p^2)^2-4M^2m_p^2}/2W$. The corresponding energies of the initial and final protons can be calculated as follows: $E_1=(W^2+Q^2+m_p^2)/2W$ and $E_2=(W^2-M^2+m_p^2)/2W$. Then $(-t_{min})=2(E_1E_2-p_1p_2-m_p^2)$ and $(-t_{max})=2(E_1E_2+p_1p_2-m_p^2)$.

Appendix C: A Model for Vector Meson Electroproduction.

Following [31] the differential cross section for the vector meson production may be expressed in terms of σ_T and σ_L cross sections corresponding to transverse and longitudinal photons:

$$\frac{d^2\sigma}{dQ^2 d\nu dt} = \frac{m_p d^2\sigma}{W dQ^2 dW dt} = \frac{\alpha(W^2 - m_p^2)}{4\pi E^2 m_p Q^2 (1-\epsilon)}\left(\frac{d\sigma_T}{dt} + \epsilon\frac{d\sigma_L}{dt}\right),$$

where $\epsilon = [1 + 2\frac{\nu^2+Q^2}{4E(E-\nu)-Q^2}]^{-1}$.

The diffractive contribution is a parametrization of the data for $Q^2 = 0$:

$$\frac{d\sigma^D}{dt} = \frac{p(0)}{p(Q^2)}(1+\epsilon R)\frac{m_\omega^4}{(Q^2+m_\omega^2)^2}\left(1 + \frac{1.4}{E_\gamma}\right)5.68(\mu b)e^{6.3t},$$

where $p(0) = \frac{W^2-m_p^2}{2W}$ and $p(Q^2) = \frac{m_p\sqrt{\nu^2+Q^2}}{W}$ are the γ momenta in the hadron C.M.S. frame, ($W \cdot p(Q^2)$ and $W \cdot p(0)$ are the flux factors for off-shell and on-shell reactions respectively), $E_\gamma = \frac{W^2-m_p^2}{2m_p}$, and $R = \xi^2\frac{Q^2}{m_\rho^2}$ ($\xi^2 = 0.4$).

Following [7] the OPE contribution can be written as:

$$\frac{d\sigma^\pi}{dt} = A\frac{2(B-C)^2 - DQ^2}{2C} + \epsilon A\frac{DQ^2}{C},$$

where

$$D = [W^2 ut - t(m_p^2+Q^2)(m_p^2-m_\omega^2) - m_p^2(Q^2+m_\omega^2)^2]/4,$$

with $u = 2m_p^2 - Q^2 + m_\omega^2 - t - W^2$,

$$C = [(W-m_p)^2 + Q^2][(W+m_p)^2 + Q^2]/4,$$

$$B = -Q^2(t-2m_p^2)/2 + (m_p^2 - Q^2 - W^2)(m_p^2 + m_\omega^2 - W^2 - t)/4,$$

$$A = 14.6\frac{6\pi\Gamma_{\omega\pi\gamma}m_\omega^3}{p(0)p(Q^2)W^2(m_\omega^2-m_\pi^2)^3}\frac{-t}{(t-m_\pi^2)^2}\frac{m_\rho^4}{(Q^2+m_\rho^2)^2}F_\omega F_N,$$

with $\Gamma_{\omega\pi\gamma} = 0.9$ MeV (recent measurements show $\Gamma_{\omega\pi\gamma} = 0.72$) being the partial width for $\omega \to \pi\gamma$ decay, and F_N, F_ω are form-factors for πN and $\gamma\pi\omega$ vertices, respectively:

$$F_N = [m_p^2 + 8.41m_\pi^2(m_\pi^2/4 - m_p^2)]/[m_p^2 + 8.41t(t/4 - m_p^2)],$$

$$F_\omega = V(2.3P_\omega(Q^2))/V(2.3P_\omega(0)),$$

with $P_\omega(0) = \frac{m_\omega^2-m_\pi^2}{2m_\omega}$ and $P_\omega(Q^2) = \frac{\sqrt{(m_\omega^2-t+Q^2)^2/4+Q^2t}}{m_\omega}$ are γ momenta in the ω rest frame, and $V(x) = [\frac{2x^2+1}{8x^2}log(4x^2+1) - 0.5]/x^4$.

References

1) S.Godfrey and N.Isgur, Phys.Rev. **D32** (1985) 189.

2) N.Cabibbo and L.Radicati, Phys.Lett.**19** (1966) 697.

3) L.J.Lanzerotti et al., Phys.Rev. **166** (1968) 1365.

4) ABBHHM Collaboration, Phys.Rev. **175** (1968) 1669.

5) J.Ballam et al., Phys.Rev. **D5** (1972) 545.
J.Ballam et al., Phys.Rev. **D7** (1973) 3150.

6) G.E.Gladding et al., Phys.Rev. **D8** (1973) 3721.

7) P.Joos et al., Nucl.Phys. **B113** (1976) 53.
P.Joos et al., Nucl.Phys. **B122** (1977) 365.

8) S.Bartalucci et al., Nuovo.Cim. **44** (1978) 587.

9) C.del Papa et al., Phys.Rev. **D19** (1979) 1303.

10) T.H.Bauer et al., Rev.Mod.Phys. **50** (1978) 261.

11) D.G.Cassel et al., Phys.Rev. **D24** (1981) 2787.

12) W.D.Shambroom et al., Phys.Rev. **D26** (1982) 1.

13) I.Cohen et al., Phys.Rev. **D25** (1982) 634.

14) D.Aston et al., Nucl.Phys. **B209** (1982) 56.

15) E.Paul, Nucl.Phys. **A446** (1985) 203.

16) J.J.Aubert et al., Phys.Lett. **161B** (1985) 203.

17) J.Busenitz et al., Phys.Rev. **D40** (1989) 1.

18) Y.Eisenberg et al., Phys.Rev. **D5** (1972) 15.

19) M.Atkinson et al., Phys.Lett. **138B** (1984) 459.
M.Atkinson et al., Nucl.Phys. **B231** (1984) 15.
M.Atkinson et al., Nucl.Phys. **B243** (1984) 1.

20) H.H.Bingham et al., Phys.Lett. **41B** (1972) 635.

21) M.Davier et al., Nucl.Phys. **B58** (1973) 31.

22) P.Schacht et al., Nucl.Phys. **B81** (1974) 205.

23) J.Ballam et al., Nucl.Phys. **B76** (1974) 375.

24) G.Alexander et al., Phys.Lett. **57B** (1975) 487.

25) M.S.Atiya et al., Phys.Rev.Lett. **43** (1979) 1691.

26) D.Aston et al., Phys.Lett. **92B** (1980) 215.
D.Aston et al., Nucl.Phys. **B189** (1981) 15.

27) K.Abe et al., Phys.Rev.Lett. **53** (1984) 751.

28) M.Atkinson et al., Phys.Lett. **127B** (1983) 132.
M.Atkinson et al., Zeit.Phys. **C26** (1985) 499.

29) G.T.Condo et al., Phys.Rev. **D43** (1991) 2787
30) H.Fraas and D.Schildknecht, Nucl.Phys. **B14** (1969) 543.
31) H.Fraas, Nucl.Phys. **B36** (1972) 191.
32) K.Schilling and G.Wolf, Nucl.Phys. **B61** (1973) 381.
33) P.J.Biggs et al.,Phys.Rev.Lett., **24** (1970) 1201.
34) H.Alvensleben et al., Phys.Rev.Lett., **27** (1971) 888.
35) P.Langacker, Phys.Rev. **D20** (1979) 2983.
36) G.Alexander et al., Phys.Lett. **57B** (1975) 487.
37) G.Wolf, Phys.Rev. **182** (1969)1538.
38) I.G.Aznauryan and K.A.Oganessyan, Phys.Lett. **249B** (1990) 309.
39) M.F.Gari and W.Krumpelmann, Phys.Rev. **D45** (1992) 1817.